Acta Biomaterialia 203 (2025) 256–276

Contents lists available at ScienceDirect

Acta Biomaterialia

journal homepage: www.elsevier.com/locate/actbio

Full length article

A costal-cartilage derived stem cell-laden prominin-1-derived peptide collagen hydrogel for angiogenesis and bone regeneration

Chenhui Cai [a,1], Rui Zuo [a,1], Zaoqing Zhang [a], Haoke Li [a], Zhongyi Liu [a], Xu Zhao [a], Mohamed EL-Newehy [c], Meera Moydeen Abdulhameed [c], Zhengchao Yuan [b,*], Xiumei Mo [b,*], Tongwei Chu [a,*], Chao Zhang [a,*]

[a] Department of Orthopedics, Xinqiao Hospital, Third Military Medical University (Army Medical University), Chongqing 400037, China
[b] State Key Laboratory for Modification of Chemical Fibers and Polymer Materials, Shanghai Engineering Research Center of Nano-Biomaterials and Regenerative Medicine, College of Chemistry, Chemical Engineering and Biotechnology, Donghua University, Shanghai, 201620, China
[c] Department of Chemistry, College of Science, King Saud University, P.O. Box 2455, Riyadh 11451, Saudi Arabia

ARTICLE INFO

Keywords:
Costal-cartilage derived stem cells
VEGF
Peptide
Collagen hydrogel
Bone regeneration
Angiogenesis

ABSTRACT

Addressing bone injury repair remains a significant challenge in clinical settings, as effective regeneration of healthy bone tissue requires simultaneous promotion of both osteogenesis and angiogenesis. Costal cartilage, being the most abundant cartilage tissue in the human body, shares structural similarities and prolonged cartilaginous properties with long bone growth plates. Its potential as a seed cell source for bone repair, however, remains unexplored. Vascular endothelial growth factor (VEGF), a key factor in bone regeneration, suffers from a short half-life and limited retention at the bone defect area, restricting its therapeutic use. In this study, a collagen hydrogel embedded with costal-cartilage-derived stem cells (CDSCs) and prominin-1-derived peptide (PR1P) was engineered to enhance endogenous VEGF recruitment. CDSCs demonstrate a strong proliferation capacity within bone defect environments, showing significant potential for bone repair. The sustained release of PR1P facilitates in situ VEGF recruitment to enhance angiogenesis and create an optimal osteogenic microenvironment for CDSCs but also demonstrates a modulatory inhibitory effect on osteoclast differentiation. In vivo application of this CDSC-laden PR1P hydrogel significantly accelerated femoral defect healing through synergistic enhancement of osteogenesis, angiogenesis, and suppression of osteoclast activity. Collectively, the study presents a promising approach to bone defect repair, underscoring the potential of CDSCs-based tissue engineering for clinical translation.

Statement of significance: Costal cartilage is the richest cartilage tissue in the human body. Our previous research isolated costal-cartilage-derived stem cells (CDSCs) and confirmed their potential for multilineage differentiation and in situ regeneration. This study further demonstrated CDSCs' significant potential for bone repair. A collagen hydrogel embedded with CDSCs and prominin-1-derived peptide (PR1P) was engineered. CDSCs demonstrate self-renewal capacity within bone defect environments. The sustained release of PR1P facilitates in situ VEGF recruitment, enhancing angiogenesis and creating an optimal osteogenic microenvironment. Additionally, the composite hydrogel has an inhibitory effect on osteoclastogenesis. Transplantation of this composite hydrogel enhanced femoral defect healing in mice by promoting both bone formation and vascular regeneration and suppressing osteoclastogenesis, presenting a promising strategy for bone defect repair.

1. Introduction

Bone defects are frequent complications associated with various conditions, including pathological fractures, inflammation, infection, and bone tumor resection [1]. Despite the inherent regenerative capabilities of human bone, addressing bone defects remains a considerable clinical challenge [2].

Conventional methods, such as autogenous and allogeneic bone transplantation, are commonly used to treat these defects [3]. However, the limited availability of autogenous bone and complications at the donor site pose significant limitations. While allogeneic bone offers a

* Corresponding authors.
E-mail addresses: yuanzhengchao2021@163.com (Z. Yuan), xmm@dhu.edu.cn (X. Mo), chutongwei@tmmu.edu.cn (T. Chu), tmmuzc@tmmu.edu.cn (C. Zhang).
[1] These authors contributed equally to this work.

https://doi.org/10.1016/j.actbio.2025.07.023
Received 12 March 2025; Received in revised form 1 July 2025; Accepted 9 July 2025
Available online 10 July 2025

Abbreviation

VEGF	vascular endothelial growth factor
CDSCs	costal-cartilage-derived stem cells
PR1P	prominin-1-derived peptide
BMSCs	bone marrow mesenchymal stem cells
ADSCs	adipose-derived mesenchymal stem cells
SSCs	skeletal stem cells
BTI	bone-tendon interface
HUVECs	human umbilical vein endothelial cells
FBS	fetal bovine serum
T20 UMC	top 20 untargeted metabolomic components
GO	Gene Ontology
KEGG	Kyoto Encyclopedia of Genes and Genomes
DEGs	differentially expressed genes
SEM	scanning electron microscopy
ALP	alkaline phosphatase
ARS	alizarin red
S-O	Safranin O/Fast Green
RUNX2	runt-related transcription factor 2
OCN	osteocalcin
COL1A1	collagen type I alpha 1
Ct.Th	cortical thickness
BMD	bone mineral density
FAK staining	focal adhesion kinase staining

wider material supply, it introduces unresolved issues, such as infection, bone resorption, nonunion, and fracture of the graft [4]. In response to these challenges, tissue engineering has become a promising alternative for bone reconstruction [5].

Bone tissue engineering, which seeks to regenerate bone tissue closely resembling natural bone, is rapidly advancing within regenerative medicine [6]. This approach integrates three key components: seed cells, growth factors, and scaffold materials. By combining biomaterials with seed cells under the influence of osteogenic factors, these cells differentiate into osteoblasts, facilitating bone regeneration [7,8].

The identification of suitable seed cells remains critical for the effective treatment of bone defects [9]. Over the years, mesenchymal stem cells from sources such as bone marrow (BMSCs) and adipose tissue (ADSCs) have been explored as seed cells [10]. BMSCs, due to their superior osteogenic properties, are considered ideal for treating bone defects. However, their clinical application is hindered by limitations in availability, proliferation capacity, and low post-transplant survival rates [11]. ADSCs, on the other hand, have garnered attention in regenerative medicine due to their abundant sources, ease of isolation, low immunogenicity, and multipotent differentiation potential [12]. Nonetheless, their strong adipogenic tendency and limited osteogenic differentiation restrict their effectiveness in bone defect repair [13]. As a result, there is still no universally suitable stem cell source for widespread clinical use.

A recent study by Chan et al. has shed light on skeletal lineage dynamics through single-cell analysis and lineage-tracing methods [14]. At the top of this hierarchy lies a small population of skeletal stem cells (SSCs), predominantly located beneath the growth plate or within the periosteum, which plays crucial roles in skeletal tissue maintenance, repair, and regeneration [15]. The growth plate itself consists of four distinct zones, with resting zone stem cells occupying the apex of the skeletal lineage [16]. These cells retain the capacity for long bone growth and maintain a cartilaginous state for an extended period prior to adulthood [17].

Costal cartilage, recognized as the richest cartilaginous tissue in the human body, exhibits structural and long-term cartilaginous characteristics that closely resemble those of long bone growth plates [18,19]. Notably, no reports have documented primary malignant tumors arising from costal cartilage [20,21]. Prior studies have successfully isolated costal-cartilage-derived stem cells (CDSCs) and confirmed their potential for multilineage differentiation and in situ regeneration. Furthermore, CDSCs demonstrated survival, proliferation, and differentiation into osteocytes, chondrocytes, and tenocytes following transplantation, ultimately regenerating bone-tendon interface (BTI) structures [22]. These results demonstrate that CDSCs may serve as promising seed cells for bone defect repair.

Angiogenesis plays a critical role in bone regeneration, with vascular endothelial growth factor (VEGF) being a critical regulator of both angiogenesis and osteogenesis [23]. As the most potent inducer of angiogenesis, VEGF functions by attracting vascular endothelial cells to bone defect sites, while also promoting the osteogenic differentiation of BMSCs [24,25]. The development of bone biomaterials capable of sustained VEGF release at the site of injury could significantly enhance bone tissue repair. However, VEGF's high molecular weight and short half-life complicate its synthesis and incorporation into biomaterials, and its rapid degradation or elution from injury sites further diminishes its therapeutic potential [26–28].

An alternative approach involves the in situ recruitment of VEGF at bone defect sites. Prominin-1-derived peptide (PR1P), a new 12-amino acid sequence (DRVQRQTTTVVA) derived from the extracellular VEGF-binding domain of prominin-1, immobilizes VEGF via hydrogen bonding [29,30]. In vitro and in vivo experiments have indicated PR1P's ability to recruit VEGF and enhance its pro-angiogenic effects [31]. Our previous research introduced electrospun poly/gelatin-based bandages encapsulated with PR1P, which effectively promoted multifunctional wound regeneration through VEGF recruitment [32]. Based on these researches, it was hypothesized that PR1P-mediated in situ VEGF recruitment could similarly enhance bone tissue regeneration, promoting angiogenesis and creating an optimal microenvironment for CDSCs to differentiate osteogenically via VEGF signaling.

Collagen hydrogels, primarily composed of type I collagen, are broadly utilized in regenerative medicine due to their superior biocompatibility, cost-effectiveness, and availability [33,34].

This study successfully developed a CDSC-laden PR1P collagen hydrogel designed to enhance bone regeneration by promoting both angiogenesis and osteogenesis and inhibiting osteoclastogenesis. Initially, the morphology, structure, and mechanical properties of the CDSC-laden PR1P hydrogel were characterized. Subsequently, the cytocompatibility and osteogenic induction capacity of the hydrogel were evaluated in vitro, followed by an investigation of its pro-angiogenic effects on HUVECs through VEGF recruitment. Osteoclasts also play a pivotal regulatory role in bone remodeling [35]. Furthermore, our experimental data revealed that the composite hydrogel exerted a discernible inhibitory effect on osteoclastogenesis, which aligns with its role in modulating bone remodeling processes. Finally, femoral defect models were used to assess in situ bone regeneration post-hydrogel transplantation. Our results confirmed that CDSCs are effective seed cells for bone tissue engineering, and the CDSC-laden PR1P hydrogel—capable of enhancing both angiogenesis and osteogenesis and suppressing osteoclastogenesis—represents a promising biomaterial for bone defect repair.

2. Materials and methods

2.1. Cell culture

C57BL/6-H11 em1Cin(CAG-loxP-ZsGreen-loxP-tdTomato)/Nju mice (referred to as ZsGreen mice) were obtained from GemPharmatech

(Jiangsu, China). Neonatal ZsGreen mice were euthanized via cervical dislocation, and the costal cartilage was aseptically isolated, removing as much soft tissue and bone marrow as possible. The tissue was digested with 0.2 % type II collagenase at 37 °C and 80 rpm for 35 min. Peripheral soft tissue was then removed by flushing with PBS. Following a second digestion with 0.2 % type II collagenase for 50 min, the costal cartilage was washed twice with PBS and blown into a single-cell suspension. The resulting cells were cultured in DMEM/F12 medium supplemented with 10 % fetal bovine serum (FBS) and incubated at 37 °C. After 24 h, non-adherent cells were discarded, and the remaining adherent cells were designated as passage 0 (P0). Human umbilical vein endothelial cells (HUVECs), sourced from Procell (Wuhan, China), were cultivated in DMEM with 10 % FBS and 1 % penicillin/streptomycin. RANKL and M-CSF were purchased from ABclonal Technology (Wuhan, China). Bone marrow monocytes/macrophages (BMMs) were harvested from femurs or tibiae of 4–6-week-old mice and subsequently cultured for 48 h in α-MEM (10 % FBS, 1 % P/S, and 50ng/mL M-CSF) for 48 h. Then BMMs were cultured in M-CSF (50 ng/mL) and RANKL (100 ng/mL) for a 5-day induction period to promote osteoclastogenesis.

2.2. Fabrication of PR1P collagen hydrogel encapsulated with CDSCs

Sprague-Dawley (SD) rats aged 4 weeks were anesthetized using 10 % chloral hydrate and euthanized by cervical dislocation. The tail was excised, and the epidermis was carefully removed. The tail tendon was isolated using forceps and washed with saline. The tendon tissue was finely minced with scissors and dissolved in 0.5 % acetic acid for 24–48 h at 4 °C. After centrifugation at 9000 rpm, the supernatant was collected, and collagen was precipitated by adding 10 % NaCl solution. Following a second centrifugation at 9000 rpm, the supernatant was discarded, and the collagen at the bottom was dissolved in 0.1 M HCl (diluted with DMEM/F12 medium) and stored at 4 °C for later use. To encapsulate PR1P (amino acid sequence: DRVQRQTTTVVA, China Peptides, Shanghai, China) into the hydrogel, 100 μg of PR1P was loaded into 1 mL of collagen to prepare a 100 μg/mL collagen solution. The CDSC suspension was added to the collagen solution to reach a cell concentration of 1×10^7 cells/mL. After mixing the short peptide and CDSCs with the collagen, NaOH solution was used to adjust the pH to 7. The collagen solution (pre-gel) was then incubated at 37 °C for 6–8 min to form the PR1P-collagen hydrogel encapsulating the CDSCs.

2.3. Untargeted metabolomics analysis of collagen hydrogel and integrative analysis of potential targets

Untargeted metabolomics analysis of the collagen hydrogel was conducted by Hangzhou Kaitai Biotechnology Co., Ltd. (Hangzhou, China). Briefly, an appropriate amount of collagen hydrogel was placed into a 1.5 mL centrifuge tube, followed by the addition of 500 μL methanol containing 2-chloro-L-phenylalanine (4 ppm). The sample was vortexed for 30 s and subsequently ground with a tissue grinder for 60 s. The sample was then subjected to 15 min of ultrasound, followed by centrifugation at 11,000 rpm at 4 °C for 8 min. The supernatant was filtered through a 0.22 μm membrane and analyzed using Liquid Chromatography-Mass Spectrometry. The LC analysis was conducted with a Vanquish UHPLC System (Thermo Fisher Scientific, USA), while metabolite detection was conducted on a Q Exactive mass spectrometer (Thermo Fisher Scientific, USA).

For data processing, raw data were converted into mzXML format through MSConvert within the ProteoWizard software package. The data were then processed in R through XCMS for feature detection, retention time correction, and alignment [36,37]. Metabolite identification was based on accurate mass and MS/MS data matched against HMDB, MassBank, LipidMaps, McCloud, KEGG, and a metabolite database developed by Panomix (Suzhou, China).

2.4. Integrative analysis of potential targets

The molecular structures of the top 20 untargeted metabolomic components (T20 UMC) were retrieved from the results of the untargeted metabolomics analysis and the PubChem database. Following established methods, the molecular structures of T20 UMC were combined with the keywords "bone regeneration" for querying GeneCards, the Therapeutic Target Database (TTD), and Online Mendelian Inheritance in Man (OMIM) databases to identify potential target genes of the collagen hydrogel [38,39]. A Venn diagram was used to visualize the intersection of potential target genes, which were then subjected to Protein-Protein Interaction (PPI) network analysis, Gene Ontology (GO) functional analysis, and KEGG pathway enrichment analysis. Protein interactions of the intersecting targets were analyzed through the STRING database, while GO and KEGG enrichment analyses were conducted through the DAVID database.

2.5. Scanning electron microscopy (SEM)

Following gelation, CDSC-laden hydrogels (with or without PR1P) were flash-frozen in liquid nitrogen and lyophilized for 48 h using a vacuum freeze dryer pre-cooled to −80 °C. The microstructure of the lyophilized hydrogels was examined by scanning electron microscopy (SEM) (Phenom, Shanghai, China) after the samples were cut into rectangular cross-sections measuring 2 mm × 2 mm.

2.6. Mechanical properties of the hydrogel

A universal material testing machine (Instron 5567, Shanghai, China) was employed to assess the unconfined compressive strength of the hydrogels. Testing was performed with a 200 N load cell at strains of 0 %, 30 %, 50 %, 70 %, and 85 %, with a crosshead rate of 5 mm/min. The compressive modulus was determined from the linear region corresponding to an initial 5 % strain ($n = 6$). The maximum strength value was derived from the stress-strain curve.

2.7. Dry/wet mass ratio

The prepared hydrogel was dissolved in deionized water at 37 °C, and excess surface water was removed using filter paper. The mass of the dissolved hydrogel (Ws) was then accurately measured. Subsequently, the hydrogel was freeze-dried, and the freeze-dried mass (Wd) was also precisely recorded. The dry-to-wet mass ratio was calculated using Formula (1) ($n = 6$).

$$Dry \Big/ wet\ mass\ ratio = \frac{W_d}{W_s} \times 100\% \quad (1)$$

2.8. Release behavior of the hydrogel

To evaluate the release behavior of the hydrogel, Rhodamine B-labeled PR1P was incorporated into the hydrogel. Cylindrical hydrogels (10 mm in diameter, 10 mm in height), containing 100 μg of Rhodamine B-labeled PR1P, were immersed in 50 mL PBS and incubated at 37 °C. At predetermined time points, 1 mL of the incubation solution was retrieved and replaced with a fresh buffer. The retrieved solution was analyzed at 549 nm using a UV1800 spectrophotometer (Thermo Fisher Scientific), and the concentration of PR1P released from the hydrogel was calculated based on a standard curve.

2.9. Degradation behavior of the hydrogel

The in vitro degradation of the collagen hydrogel was evaluated by immersing equal volumes of hydrogel samples into a PBS buffer solution and oscillating them at 37 °C. At specific time intervals, the hydrogel samples were removed, rinsed with deionized water, freeze-dried, and

weighed. The remaining mass of the hydrogel was calculated using Formula (2) ($n = 6$), where Wt represents the weight of the hydrogel at a given time point, and W0 represents the initial hydrogel weight.

$$Remained\ mass = \frac{W_t}{W_0} \times 100\% \quad (2)$$

2.10. Rheological testing of the hydrogel

Rheological properties were tested using a rotating rheometer (DHR-3, TA, USA). Cylindrical hydrogels were placed on parallel plates (φ = 10 mm; height = 5 mm) at 37 °C. The frequency range was set to 1–100 rad/s, with a constant strain of 1.0 %. The storage modulus (G′) and loss modulus (G″) were recorded across the frequency range.

2.11. Cell viability

1×10^4 CDSCs were encapsulated in collagen hydrogel loaded with different gradient concentrations of PR1P (0, 0.5, 1, 10, 100 μg/ml). In vitro 3D culture was then performed on the hydrogel by immersing it in DMEM/F12 for 3 and 7 days (n = 6). For the CCK-8 experiment, each well was treated with 10 μL of CCK-8 solution (Dojindo, Kumamoto, Japan). The absorbance at 450 nm was measured after 2 h of incubation at 37 °C in a humidified environment with 5 % CO2. For the focal adhesion kinase staining (FAK staining) assay, cells were washed twice with wash buffer and permeabilized with Triton X-100 after 30 min of fixation with 4 % paraformaldehyde at 37 °C. Cells were then blocked with goat serum for 25 min. Then we washed the cells twice with PBS again after they had been stained with tetramethylrhodamine-conjugated phalloidin for 1.5 h. DAPI was used to counterstain the nuclei. Fluorescence microscopy was used to visualize fluorescence images.

2.12. VEGF recruitment in vitro

To prepare a standard VEGF solution, 2 nanograms of VEGF 165 protein (Sino Biological, Beijing, China) were dissolved in 1 mL PBS containing 2 % BSA, resulting in a VEGF concentration of 2 ng/mL. Collagen hydrogels (8 mm × 8 mm × 8 mm) loaded with PR1P at gradient concentrations (1, 10, 100 μg/mL) were immersed in the VEGF solution and incubated at 37 °C for 8 h. After rinsing the hydrogel three times with PBS, VEGF-bound PR1P hydrogels were transferred to centrifuge tubes containing 10 mL DMEM and incubated at 37 °C for 24 h to collect the VEGF-recruited PR1P hydrogel extract. The concentration of VEGF in the extracted medium was measured using a VEGF ELISA Kit (Solarbio, Beijing, China).

2.13. Induction and identification of osteogenic differentiation

CDSCs were seeded at a density of 1×10^5 cells/well in a 24-well plate and allowed to reach confluence. Osteogenic induction was conducted by adding a 750 μl osteogenic differentiation medium (Cyagen, USA) to each well. We changed the culture medium every three days. After 14 days of induction, the total RNA of CDSCs was extracted and subjected to RT-qPCR. Additionally, a part of CDSCs was used for alkaline phosphatase (ALP) staining following the ALP staining kit (Beyotime, Shanghai, China) instructions. After 21 days of induction, an alizarin red staining (ARS) kit (Beyotime, Shanghai, China) was used to observe the calcium nodules generated by the CDSCs.

2.14. RNA extraction and qRT-PCR

TRIzol buffer was used to obtain RNA, and NanoDrop ND-1000 microplate readers were used to determine RNA concentrations. cDNA was reverse transcribed using PrimeScript TM RT reagent kit (Takara, Japan). Then cDNA was subjected to qRT-PCR using SYBR Green PCR Mix (Takara, Japan). The expression of runt-related transcription factor 2 (RUNX2), osteocalcin (OCN), collagen type I alpha 1 (COL1A1), and ALP was measured, using GAPDH as a reference. **Supplementary Table S1** lists primer sequences.

2.15. Western blot

Following total protein extraction, samples were electrophoresed by SDS-PAGE gels and transferred to PVDF membranes. The membranes were blocked with 4 % BSA for 2 h, then incubated overnight at 4 °C with specific primary antibodies including RUNX2 (1:1000, Beyotime), Osterix (1:500, Santa Cruz), OCN (1:1000, ABclonal), VEGF (1:1000, ABclonal), NFATc1 (1:5000, Proteintech), C-Fos (1:5000, Proteintech), MMP9 (1:1500, Proteintech) and GAPDH (1:5000, Proteintech). After TBST washing, membranes were probed with HRP-conjugated secondary antibodies for 1.5 h. Protein signals were visualized using an ECL substrate and imaged with a Bio-Rad imaging system (CA, USA).

2.16. Assessment of endothelial cell migration and angiogenesis

To evaluate the impact of VEGF-recruited PR1P hydrogel on HUVEC migration, both wound healing and transwell assays were conducted. For the wound healing assay, HUVECs were cultivated in six-well tissue culture plates until 75–80 % confluency was achieved, and treated with 50 nmol/mL of mitomycin for four hours. Following treatment, the cells were washed twice with sterile PBS. A scratch was made in the cell monolayer of each well using sterile plastic tips, after which the cells were washed twice more with PBS and incubated with the extracted medium from the VEGF-recruited PR1P hydrogel for 24 h. Images of the cells and scratch area were taken at 0 h and 24 h, and the wound closure area was quantified by ImageJ software. A transwell assay was conducted using 8 mm transwell chambers (Corning, NY, USA). CDSCs (1×104) were seeded on Matrigel containing the hydrogel extract medium (serum-free), while the lower chamber contained 400 μL complete medium. After 3 days of incubation, we stained invading cells with 0.5 % crystal violet and counted them. To evaluate the effect of VEGF-recruited PR1P hydrogel on HUVEC angiogenesis, a tube formation assay was carried out. HUVECs at a density of 5×10^4 were seeded onto Matrigel and incubated for 6 h. The ability of the endothelial cells to form tubular networks was visualized via microscopy, and tube formation was quantified using ImageJ software ($n = 6$).

2.17. Assessment of osteoclast differentiation

Following osteoclastic induction, BMMs were subjected to TRAP staining using a commercial kit (Servicebio, China) per the manufacturer's protocol. Multinucleated cells (≥3 nuclei) were identified as mature osteoclasts. FAK staining was performed following the protocol outlined in Section 2.11. The expression of osteoclast-specific markers was subsequently analyzed through qRT-PCR and western blot analysis.

2.18. Transcriptome analysis

CDSCs encapsulated in collagen hydrogels with or without PR1P supplementation underwent 7-day osteogenic induction followed by transcriptomic profiling. Triplicate biological replicates were sequenced on an Illumina HiSeq™ 2500 platform (Sangon Biotech, Shanghai, China). Differential gene expression analysis was conducted using DEGseq (|log2FC| >1, adjusted p-value <0.05), followed by functional annotation of significant genes through Gene Ontology (GO) and KEGG pathway enrichment analyses implemented in clusterProfiler (v3.14.3).

2.19. In vivo experiments

For the in vivo study, the Hua Fukang Experimental Animal Center (Beijing, China) provided us with male C57BL/6 mice (8 weeks old). The

mice were divided randomly into three experimental groups (n = 6 for each group): (1) a control group receiving the collagen hydrogel, (2) the CDSC gel group where CDSC-laden collagen hydrogel was transplanted, and (3) the CDSC gel@PR1P group where CDSC-laden PR1P collagen hydrogel was transplanted. All surgeries were conducted by two experienced orthopedic surgeons and approved by the Ethics Committee of the Army Medical University. The mice were anesthetized via intraperitoneal injection of 2 % tribromoethanol, and the distal hindlimb was shaved. Skin and subcutaneous tissue were incised to expose the femur, which was stabilized with an intramedullary steel needle before creating a 4 mm segmental bone defect using a wire saw through two parallel osteotomies in the midshaft. Hydrogels, specific to each experimental group, were then transplanted into the defect site. The surrounding soft tissue was sutured around the femur to secure the hydrogel, followed by closure of the skin and subcutaneous tissue using 6–0 sutures.

2.20. Micro-CT scanning

At 4 weeks and 8 weeks after surgery, all animals were sacrificed. We fixed the femoral samples with 4 % paraformaldehyde after harvesting them. Micro-CT scans (Skyscan1276, Bruker, Belgium) were performed on the femurs after fixation for two days. The bone volume of the defect area, cortical thickness (Ct. Th), bone mineral density (BMD), and the cross-sectional area of the middle femur were analyzed.

2.21. Histological staining and immunohistochemistry (IHC)

Bones were decalcified in 10 % ethylenediaminetetraacetate in PBS for 10 days. All the femurs were irradiated with a 488-nm excitation light (3415RG, LUYOR, USA) and imaged. Then OCT-embedded bone tissues were sectioned into 6 μm-thick sections. DAPI, H&E, and Safranin O/Fast Green (S-O) staining were performed following the manufacturer's instructions. For immunohistochemical staining, decalcified femoral specimens were paraffin-embedded and sectioned into 4-μm-thick slices. Tissue sections were incubated at 4 °C overnight with specific primary antibodies: VEGF (1:500, ABclonal) and OCN (1:100, ABclonal), followed by 1-hour incubation with corresponding secondary antibodies. Histological and statistical analyses were subsequently performed using ImageJ software.

2.22. Immunofluorescence

Frozen sections of femurs were subjected to immunofluorescence staining. After two washes with PBS, the sections were blocked in goat serum for 30 min. They were then incubated with CD31/PECAM-1 primary antibody (1:200 dilution, AF3628, R&D, USA) overnight at 4 °C. Afterward, the sections were washed twice with PBS and incubated with fluorescent secondary antibody at room temperature for 1.5 h. After three additional PBS washes, the sections were mounted with a DAPI-containing anti-fade mounting medium and visualized under a fluorescence microscope. CD31 fluorescence was quantified via ImageJ. For each sample, 3–5 non-overlapping fields within the femoral defect (localized by DAPI-defined tissue architecture) were analyzed. The percentage of CD31-positive area was calculated. Fields from the same defect were averaged to generate a single data point per animal. Statistical comparisons between groups were performed using these animal-level data points. To exclude nonspecific staining, negative controls (secondary antibody only) were used, and only signals with endothelial-like morphology (tubular/linear structures) were included in quantification.

2.23. Statistical analysis

Data are presented as mean ± standard deviation (SD), and statistical analysis was carried out through GraphPad Prism 7.0. Normality was assessed for each dataset using the Shapiro-Wilk test. For comparisons between two groups, independent Student's *t*-tests were applied for normally distributed data; otherwise, the Mann-Whitney U test was used. For comparisons across three or more groups, one-way analysis of variance (ANOVA) was employed for parametric data, while the Kruskal-Wallis H test was utilized for non-parametric data. A p-value < 0.05 was considered statistically significant.

3. Results

3.1. Characterization of rat tail collagen hydrogel

The preparation process is illustrated in Fig. 2A, with detailed procedures described in the Methods Section. As shown in Fig. 2B, the rat tail collagen hydrogel solution in both the CDSCs Gel group and the CDSCs Gel@PR1P group appeared pink and translucent under acidic conditions due to the addition of phenolphthalein. After neutralization to pH 7 with an alkaline solution, the collagen hydrogel solution gradually gelled at 37 °C, forming a stable cylindrical hydrogel in the mold.

The microstructure of the freeze-dried rat tail collagen hydrogel was examined by SEM (Fig. 2B). The hydrogels in both groups exhibited a loose, porous structure after freeze-drying, indicating a lower content of fixative material. SEM imaging revealed a lamellar structure with numerous micropores. This interconnected porous architecture facilitates the exchange of substances between the interior and exterior of the collagen hydrogel, supporting cell growth.

The compression modulus, a key mechanical property describing the stiffness of hydrogels under compression, was evaluated for both the CDSCs Gel and CDSCs Gel@PR1P groups. Fig. 2C presents a schematic of the composite hydrogel compression testing setup. The compressive stress-strain curves indicated that the hydrogel did not fracture under compression, although water continued to exude from the structure (Fig. 2D).

The rheological properties of the collagen hydrogel were further investigated. As depicted in Fig. 2I, G' in the low-frequency range increased progressively with rising frequency, indicating superior mechanical elasticity as G' exceeded G''. However, as amplitude continued to rise, G' sharply increased until reaching the critical strain, at which point the hydrogel structure collapsed, likely due to water loss within the matrix. These results suggest that the hydrogels are prone to water loss under external stress, underscoring the need to improve their mechanical stability in future work. Additionally, the maximum strength measurements revealed that PR1P incorporation did not significantly affect the compressive modulus of the collagen hydrogel (Fig. 2E).

The average gelation times for the CDSCs Gel and CDSCs Gel@PR1P groups at 37 °C were 39.0 ± 6.5 s and 39.5 ± 5.0 s, respectively, with no statistically significant difference (Fig. 2F). The dry-to-wet mass ratios of the CDSC and CDSC@PR1P hydrogels were 0.71±0.07 % and 0.70±0.06 %, respectively, demonstrating no significant difference in water absorption between the groups ($p > 0.05$) (Fig. 2G). The low dry-to-wet mass ratio indicates a low dry matter content of the hydrogel. Further, the mechanical properties of hydrogel should be optimized and improved.

Hydrogel degradability, defined as the breakdown of the material into smaller molecules under specific physical or chemical conditions, was evaluated in vitro. After 30 days, both groups retained approximately 40 % of their initial mass, indicating that the collagen hydrogels exhibit strong stability, making them suitable for in vivo transplantation (Fig. 2H). Finally, the release profile of the CDSCs Gel@PR1P hydrogel was assessed, revealing a slow and sustained release of PR1P from the hydrogel for up to 180 h in vitro (Fig. 2J).

3.2. Network pharmacology analysis

To explore the potential of major metabolites derived from collagen hydrogel in promoting bone tissue regeneration, a network pharmacological analysis was conducted on the top 20 untargeted metabolomic

components (T20 UMC) related to "bone regeneration." The molecular structures of the T20 UMC, representing the key metabolic components of rat tail tendon collagen hydrogel, are illustrated in Fig. S1. Using the molecular structures of the T20 UMC alongside the keyword "bone regeneration," potential target genes of the composite hydrogel were identified.

As depicted in the Venn diagram (Fig. S2A), the T20 UMC and bone regeneration categories referenced 2729 and 4998 target genes, respectively, with 1094 (16.5 %) genes overlapping between the two sets. This overlap suggests that the metabolic components from the composite hydrogel hold significant potential for promoting osteogenesis.

These intersecting genes were subsequently subjected to GO and KEGG enrichment analyses through the David database. KEGG pathway analysis revealed that the shared target genes are primarily involved in signaling pathways related to osteogenesis, inflammation regulation and angiogenesis, such as the PI3K-AKT signaling pathway, AGE-RAGE signaling pathway, and TNF signaling pathway (Fig. S2B). Furthermore, GO enrichment analysis emphasized the involvement of these genes in biological functions including positive regulation of transcription, positive regulation of cell proliferation, inflammatory response, and protein binding, which were closely related to cell proliferation, metabolic activity, and inflammation regulation (Fig. S2C). In addition, we constructed a PPI network of these intersecting targets. After topological analysis, the core targets we obtained were also related to inflammation, cell proliferation and angiogenesis, such as TNF, IL-6, IL-1B, AKT1, STAT3, EGF, EGFR, NFKB1, MYC, and so on (Fig. S3). These results suggest that the metabolic components of the composite hydrogel exhibit potential for promoting bone regeneration.

3.3. Cytocompatibility evaluation of the PR1P collagen hydrogel

To evaluate the cytocompatibility of the PR1P collagen hydrogel and optimize the concentration of incorporated PR1P, the proliferation of CDSCs derived from ZsGreen mice in 3D-culture within collagen hydrogels containing varying concentrations of PR1P (0.5 μg/mL, 1 μg/mL, 10 μg/mL, and 100 μg/mL) was assessed using the CCK-8 assay (Fig 3A). On days 3 and 7, no statistical difference in cell proliferation was observed between the hydrogel group and the 0.5 μg/mL PR1P group. However, when the PR1P concentration exceeded 1 μg/mL, a concentration-dependent increase in CDSC proliferation was noted in the PR1P collagen hydrogel (Fig. 3A). Additionally, ZsGreen fluorescence intensity was observed using a fluorescence microscope, revealing a marked increase in fluorescence intensity of CDSCs as the PR1P concentration in the collagen hydrogel increased (Fig. 3B-C). To further assess the biocompatibility of the PR1P collagen hydrogel, FAK staining was performed on CDSCs treated with collagen hydrogels containing various concentrations of PR1P. Rhodamine-conjugated phalloidin was used to label F-actin in the cytoskeletal microfilaments.

As shown in Fig. 3D, CDSCs cultured on collagen hydrogels, with or without PR1P encapsulation, exhibited robust growth, a clear background, and uniform staining, indicating that the PR1P collagen hydrogel demonstrates favorable biocompatibility (Fig. 3D-E). Although no distinct differences in cell morphology were observed among the groups, the increased cell density suggested that PR1P loading supports enhanced CDSC growth and proliferation.

3.4. The ability of PR1P collagen hydrogel to recruit VEGF in vitro

To confirm that the PR1P collagen hydrogel effectively recruits endogenous VEGF as expected, an in vitro experiment was designed to examine its VEGF recruitment capability (Fig. 4A). The PR1P collagen hydrogel was incubated in a VEGF solution of specific concentration, allowing it to gradually recruit VEGF. Afterward, the hydrogel was eluted and soaked in a complete medium to obtain the extracted medium, and the VEGF concentration was measured via ELISA. All PR1P-containing collagen hydrogels effectively recruited VEGF in a dose-dependent manner. Specifically, the hydrogel containing 100 μg/mL of PR1P recruited about 27.5 ± 2.1 pg/mL of VEGF within 8 h (Fig. 4B).

3.5. Effect of PR1P collagen hydrogel on osteogenic differentiation of CDSCs

To assess the impact of PR1P collagen hydrogel on the osteogenic differentiation of CDSCs in vitro, ARS staining, ALP staining, and qRT-PCR for osteogenic marker genes were conducted. As illustrated in Fig. 4C, after osteogenic induction for 21 days, CDSCs treated with hydrogel extract displayed significantly greater calcium deposition than those without hydrogel extract, indicating the strong potential of PR1P collagen hydrogel to promote osteogenic differentiation. Similar outcomes were observed in ALP staining (Fig. 4D), where CDSCs cultured in osteogenic medium with hydrogel extract showed markedly higher ALP activity compared to those without extract after 14 days. Moreover, real-time qPCR revealed a significant upregulation of key osteogenic markers, including RUNX2, OCN, COL1A1, and ALP, in the hydrogel extract group compared to other groups (Fig. 4E-H). The above results strongly support the conclusion that PR1P collagen hydrogel effectively enhances osteogenic differentiation. The schematic of the experimental design is presented in Fig. 4I.

3.6. PR1P collagen hydrogel enhanced huvec migration and endothelial network assembly via VEGF recruitment in vitro

To further validate the effect of PR1P collagen hydrogel on enhancing HUVEC migratory capacity via VEGF recruitment, hydrogel extracts containing different concentrations of PR1P (1 μg/mL, 10 μg/mL, 100 μg/mL) were used to stimulate HUVECs, and their migration ability was examined using wound healing experiment and transwell experiment. As shown in the wound healing assay results, the wound closure area in the 10 μg/mL and 100 μg/mL PR1P groups was significantly larger than in the hydrogel group and 1 μg/mL PR1P group after 24 h. No statistical difference was observed between the hydrogel group and the 1 μg/mL PR1P group at this time point (Fig. 5A). Similar trends were found in the transwell assay, where HUVECs treated with extracts from 10 μg/mL and 100 μg/mL PR1P hydrogels exhibited stronger migration capacity than other groups (Fig. 5B).

We next evaluated the effect of PR1P hydrogel extracts on HUVEC endothelial network assembly capability on Matrigel, which models early stages of angiogenesis [40]. The experimental grouping and stimulation methods were consistent with the previous assays, and tube formation was observed 4–6 h post-inoculation on Matrigel. All groups demonstrated the formation of initial capillary-like networks, but the 10 μg/mL and 100 μg/mL PR1P groups showed significantly increased tubular structure formation, including a higher number of meshes and nodes, compared to the hydrogel group (Fig. 5C). Additionally, control experiments with PR1P-free collagen hydrogels (Gel) and PR1P-loaded hydrogels without VEGF exposure (Gel@PR1P) showed no significant enhancement in HUVEC proliferation, migration, or tube formation compared to DMEM baseline (Fig. S4). These findings collectively demonstrate that PR1P-functionalized hydrogel extracts promote VEGF-dependent HUVEC migration and endothelial network assembly in vitro, key early events in vascular morphogenesis that precede lumen formation.

3.7. PR1P collagen hydrogel suppressed osteoclastogenesis in vitro

Furthermore, given the critical regulatory role of osteoclasts in bone homeostasis, we systematically evaluated the biological efficacy of PR1P collagen hydrogel in modulating osteoclast differentiation. First, CCK-8 assays demonstrated that the hydrogel extracts of PR1P collagen hydrogel (PR1P concentrations ≤100 μg/mL) exhibited no significant cytotoxicity toward osteoclasts (Fig. 6A). Subsequently, TRAP staining

of BMMs demonstrated a PR1P-concentration-dependent attenuation of osteoclastogenesis by the hydrogel extracts, as delineated in Fig. 6B, D, and E. Then, BMMs undergoing osteoclastic induction were exposed to hydrogel extracts containing gradient concentrations of PR1P. FAK staining revealed a marked pharmacological attenuation of F-actin ring formation and multinucleated osteoclast development upon hydrogel extract treatment (Fig. 6C, F, and G). Furthermore, qRT-PCR analysis of RANKL-induced osteoclast differentiation revealed significant down-regulation in key osteoclastic genes (CTSK, TRAP, NFATc1, c-Fos) following hydrogel extract treatment (Fig. 6H-K). Subsequent western blot analysis corroborated dose-dependent suppression of osteoclast-specific markers by the PR1P-incorporated hydrogel extracts, demonstrating consistent pharmacological modulation at both transcriptional and translational levels (Fig. 6L). Collectively, these findings demonstrate the hydrogel extracts' inhibitory efficacy against osteoclastogenesis.

3.8. In vivo bone repair assessment

The collagen hydrogels, CDSC-laden collagen hydrogels, and CDSC-laden PR1P collagen hydrogels were surgically implanted into the mid-shaft femoral bone defects of mice to evaluate their effect on bone repair. The experimental workflow is outlined in Fig. 7A, and the detailed surgical procedure for the femoral defect model is depicted in Fig. 7B

Femurs were harvested at 4 and 8 weeks post-transplantation, and visual examination revealed that the femurs in the CDSCs gel and CDSCs gel@PR1P groups had a larger diameter and increased bone mass compared to the control group (Fig. 7C-D). Stable ZsGreen fluorescence in both CDSCs gel and CDSCs gel@PR1P groups was observed, fully covering the bone defect area, indicating that CDSCs survived and proliferated stably in the post-transplantation environment (Fig. 7C-D and Fig. S5). Notably, the fluorescence area in the CDSCs gel@PR1P group was more extensive than in the CDSCs gel group at both 4 and 8 weeks post-transplantation, suggesting enhanced survival and proliferation of CDSCs in VEGF-recruited environment (Fig. 7C-D and Fig. S5). These results demonstrate that rat tail tendon-derived collagen hydrogels exhibit favorable in vivo biocompatibility and that CDSCs encapsulated in collagen hydrogels adapt well to the post-transplantation environment.

Micro-CT scans of the femur specimens were performed to assess bone defect repair in all groups. Representative images of micro-CT reconstructions are shown in Fig. 8A-B. Treatment with CDSC-laden collagen hydrogel or CDSC-laden PR1P collagen hydrogel significantly enhanced new bone formation within the femoral defect area compared to the control group at 4 and 8 weeks post-transplantation (Fig. 8C). Additionally, the cross-sectional area of the mid-femur in the CDSCs gel and CDSCs gel@PR1P groups was significantly larger than that of the control group (Fig. 8C). Consistent with these results, the cortical thickness (Ct. Th) in the control group remained thin, and the newly formed bone was discontinuous. In contrast, the cortical bone defect area in the CDSCs gel and CDSCs gel@PR1P groups was nearly fully repaired with continuous new bone formation.

The most robust bone regeneration was observed in the CDSCs gel@PR1P group, which exhibited significantly higher bone volume, a larger cross-sectional area, and thicker cortical bone at both 4 and 8 weeks post-surgery (Fig. 8C). However, the transplantation of hydrogels did not significantly alter bone mineral density (BMD) in the defect area (Fig. 8C).

During bone defect healing, angiogenesis and osteogenesis work synergistically to drive bone regeneration [41]. The PR1P released by the CDSCs gel@PR1P in the local microenvironment likely recruited significant amounts of endogenous VEGF, promoting vascular hyperplasia and creating an optimal osteogenic environment.

Histological and immunofluorescent staining were subsequently performed to thoroughly evaluate in vivo bone repair outcomes. As shown in Fig. 9A-B and Fig. S6, both H&E and S-O staining demonstrated that the CDSCs gel and CDSCs gel@PR1P groups exhibited significantly enhanced osteogenic effects, with extensive new bone formation and thicker cortical bone compared to the control group. Although some chondrocyte-like cells persisted in the outer layer of the femur in the CDSCs-treated groups, hard callus (woven bone) gradually replaced cartilage through endochondral ossification, progressing from the outer to the inner layers. In the innermost layer, the transplanted CDSCs in both the CDSCs gel and CDSCs gel@PR1P groups underwent extensive osteogenic differentiation, resulting in the formation of mature bone cortices. In contrast, the control group still showed discontinuous and thin cortical bone (Fig. 9A-B). Furthermore, the CDSCs gel@PR1P group demonstrated the most robust healing, with the highest levels of new bone formation, as reflected by the increased cortical bone thickness, consistent with the micro-CT analysis results (Fig. 9A-B and Fig. S6).

3.9. PR1P collagen hydrogel enhances CDSCs osteogenic differentiation through VEGF signaling

To elucidate the pro-osteogenic mechanisms of the composite hydrogel, CDSCs undergoing osteogenic differentiation were treated with either VEGF-recruited collagen hydrogel or PR1P collagen hydrogel extracts for 7 days. Transcriptomic profiling revealed 273 differentially expressed genes (DEGs) between cohorts, comprising 162 significantly upregulated and 111 downregulated genes in the PR1P collagen hydrogel group versus the control group. Hierarchical clustering heatmaps and volcano plots demonstrated distinct transcriptional landscapes (Fig. 10A and Fig. S7). Subsequently, we performed a GO analysis of DEGs and visualized the results with lollipop plots and network plots. Compared to the collagen hydrogel group, the PR1P collagen hydrogel group demonstrated predominantly enrichment results associated with vascular development, including "positive regulation of angiogenesis" and "positive regulation of vasculature development" (Fig. 10B-C, Table S2). This conclusion was further corroborated by the expression heatmap of vasculature development-related genes (e.g., CCL5, PGF, WNT5A, WNT2) derived from transcriptomic analysis (Fig. 10D). The VEGF signaling pathway serves as the central regulatory mechanism for angiogenesis [23]. Notably, VEGF has been documented to potentiate osteogenic differentiation through downstream pathways including PI3K-Akt and MAPK cascades [42]. We therefore hypothesize that PR1P collagen gel may facilitate CDSC osteogenic differentiation via VEGF-mediated signaling. Western blot analysis of VEGF expression and osteogenic differentiation markers (e.g., RUNX2, OCN) provided experimental validation for this hypothesis (Fig. 10E). Concomitantly, IHC analysis of VEGF expression was performed on neoosseous regions in femoral defect models at 2 weeks post-implantation. A quantitative evaluation revealed that the CDSCs gel@PR1P group exhibited a marked enhancement in VEGF signaling intensity compared to the control group and CDSCs gel group (Fig. 10F). These findings collectively indicate that PR1P collagen hydrogel likely enhances osteogenic differentiation of CDSCs through augmentation of VEGF signaling.

3.10. Osteogenesis, angiogenesis, and osteoclastogenesis of the composite hydrogels in vivo

OCN, a pivotal marker for osteogenic maturation, orchestrates matrix deposition and mineralization during bone formation [43]. Immunohistochemical evaluation at 8 weeks post-implantation in femoral defects was performed, which demonstrated significantly elevated OCN expression in osseous repair zones of both CDSCs Gel and CDSCs Gel@PR1P groups, with the latter exhibiting the most pronounced immunoreactivity (Fig. 11A). The above findings demonstrate that CDSC-laden PR1P hydrogel significantly enhances osteogenesis within osseous defect microenvironments. Since bone is a highly vascularized tissue requiring a sufficient blood supply for proper healing,

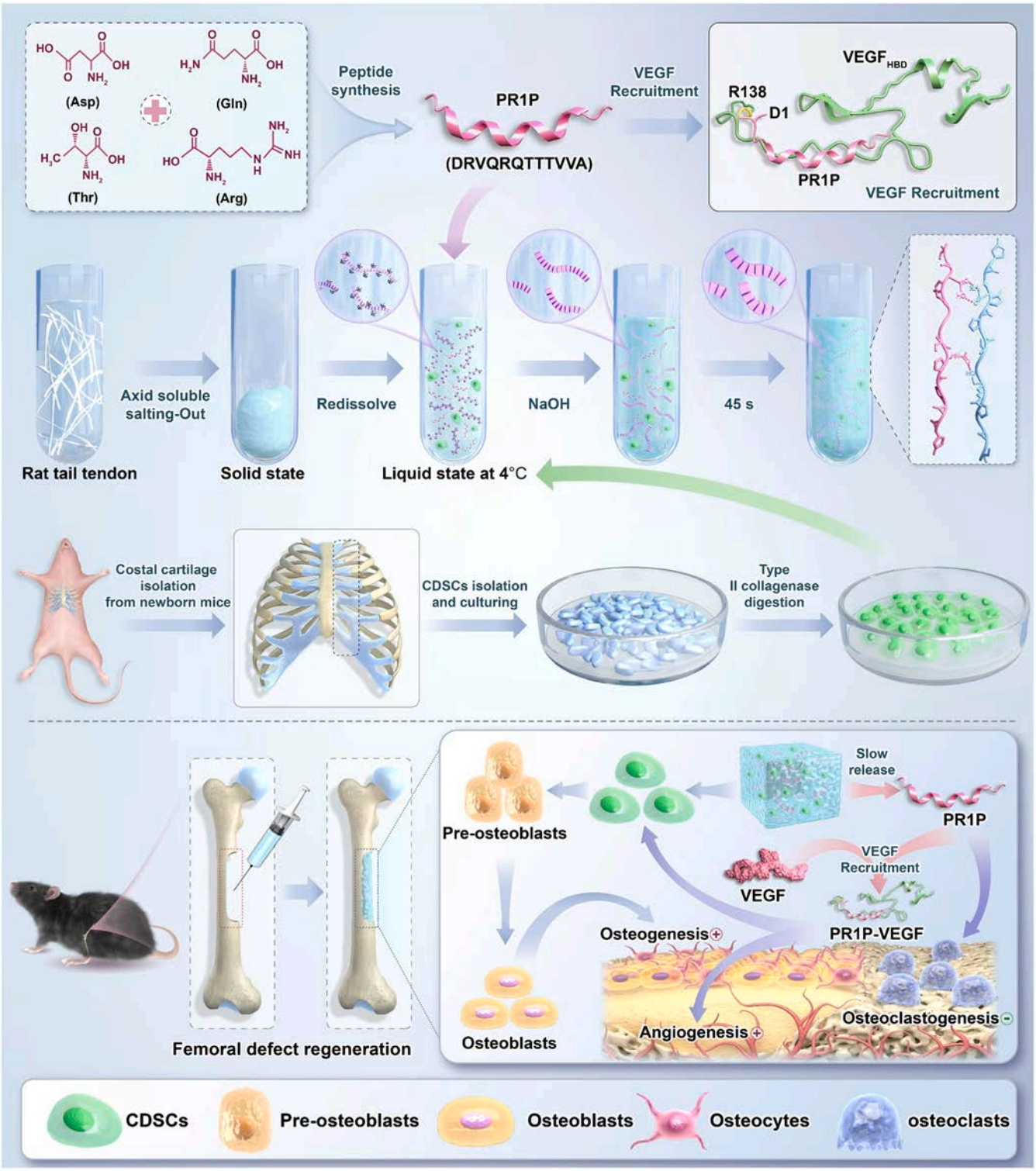

Fig. 1. The scheme of this research. CDSCs harvested from the costal cartilage of newborn ZsGreen mice and PR1P are mixed into collagen hydrogel extracted from rat tail tendons to obtain CDSC-laden PR1P collagen hydrogel. The VEGF-recruited composite hydrogel facilitates bone defect repair by promoting angiogenesis and osteogenesis and suppressing osteoclastogenesis in a mouse bone defect model.

angiogenesis is essential for bone defect repair [44]. To assess vascularized bone regeneration in the defect area, immunofluorescence staining for CD31 was performed on frozen femur sections. The staining revealed a significant increase in the total cross-sectional area of blood vessels in the CDSCs gel@PR1P group at 4 weeks post-surgery compared to the other groups, aligning with in vitro results (Fig. 11B-C). These results confirm that CDSC-laden PR1P hydrogel effectively promotes the formation of new vascular networks in the bone defect area. Finally, we evaluated the modulatory effects of the hydrogel on osteoclastogenesis within the bone repair niche. TRAP staining demonstrated that CDSCs gel@PR1P group exhibited obvious suppression of osteoclast activity in neoosseous regions compared to CDSCs Gel group and control group (Fig. 11D-E), which demonstrates that CDSC-laden PR1P hydrogel potently suppresses osteoclastogenesis within osseous defect region.

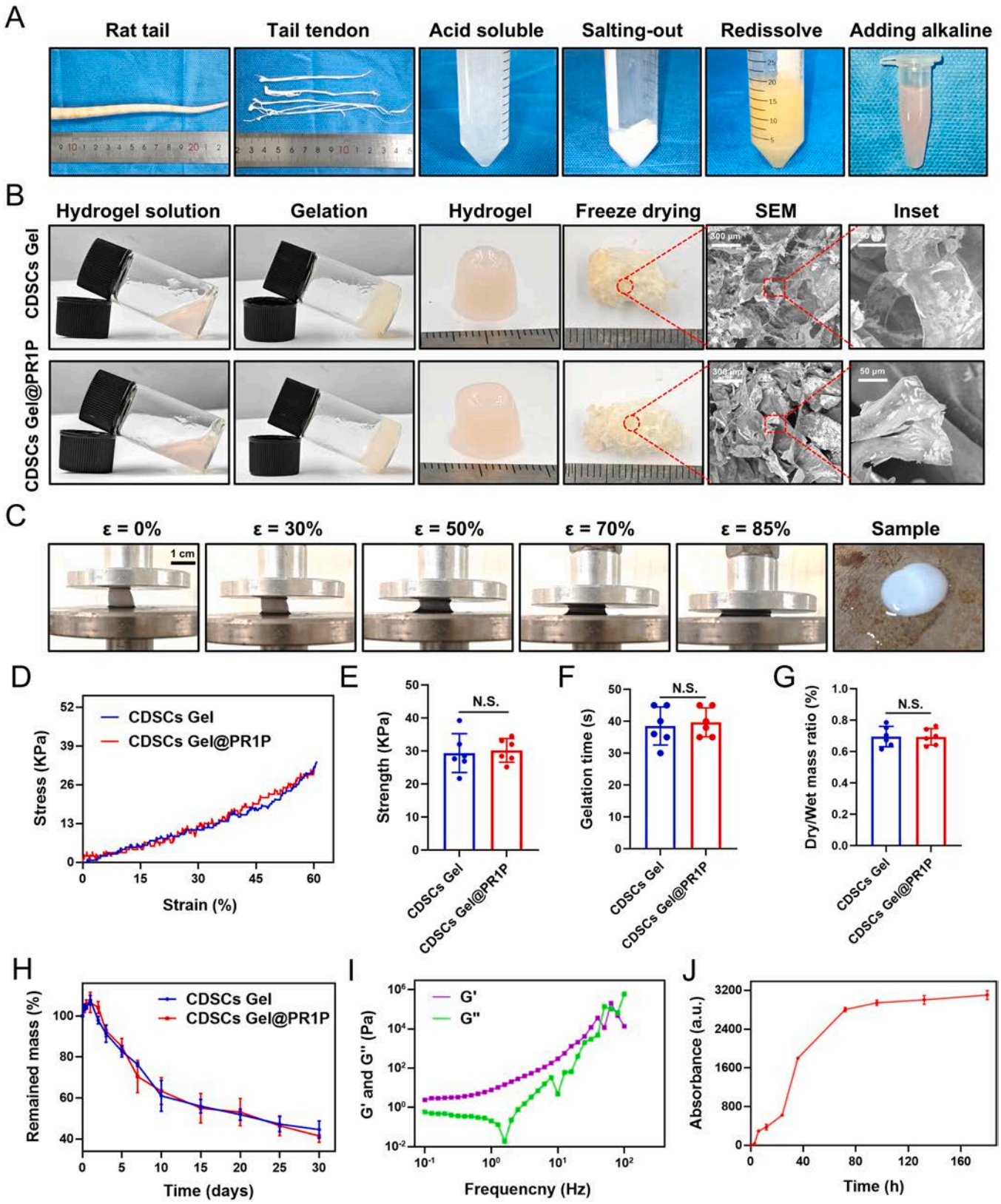

Fig. 2. Characterization of the CDSC-laden PR1P collagen hydrogel. (A) Schematic of the collagen hydrogel fabrication. (B) Morphology of the composite hydrogel before and after gelation and representative SEM images. Scale bars: 300 μm (50 μm in the inset). (C) Schematic drawing of compression testing of composite hydrogel. (D) Stress-strain curve of hydrogels. (E) The compressive modulus of composite hydrogels. (F) The average gelation time of composite hydrogels. (G) The dry/wet mass ratio of composite hydrogels. (H) The degradation properties of composite hydrogels. (I) The rheological properties of composite hydrogels. (J) The PR1P release characteristics of composite hydrogels. $^{*}p < 0.05$ compared as denoted by bar. Values are expressed as means ± SD.

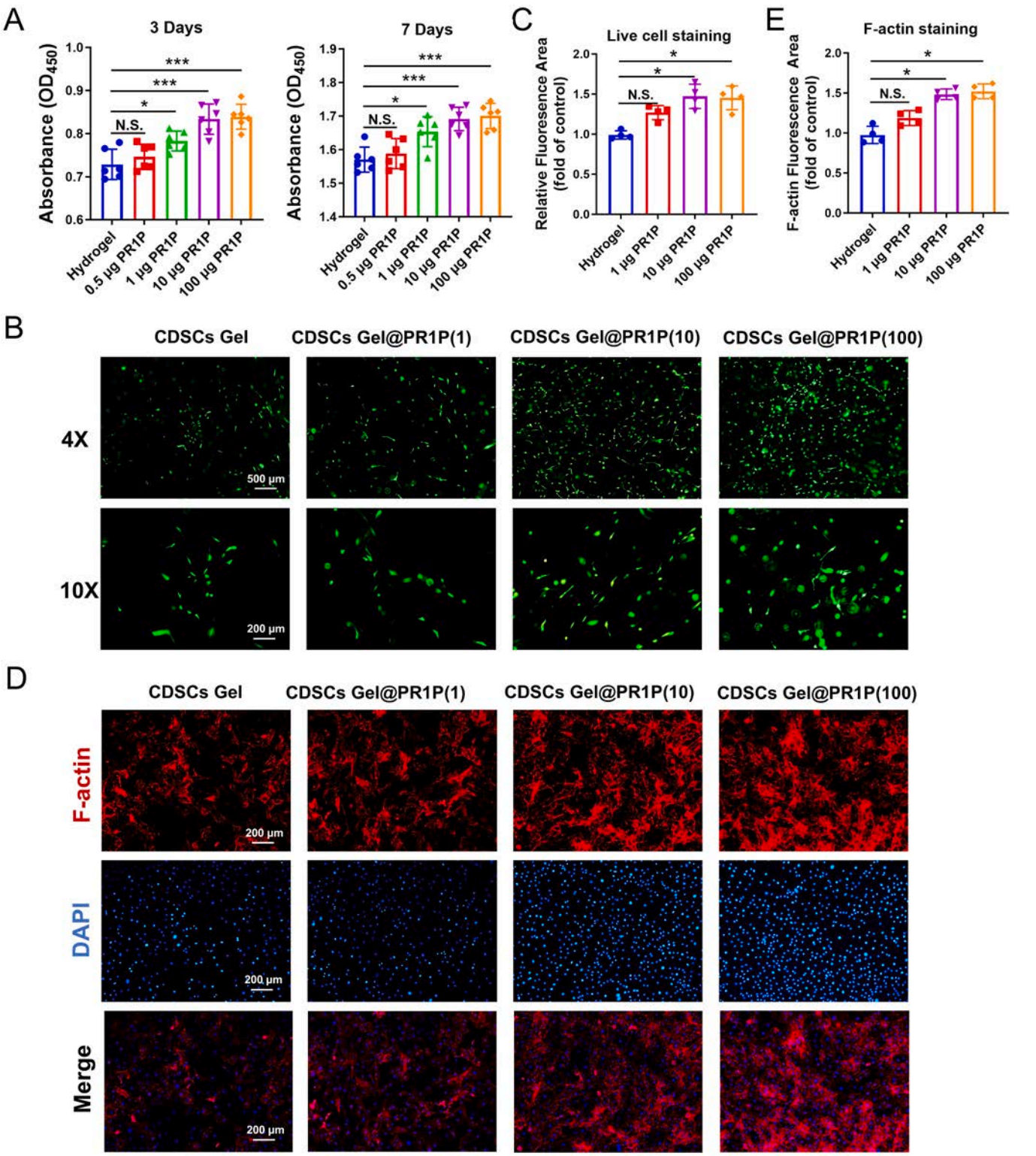

Fig. 3. Biocompatibility of composite hydrogels. (A) CCK-8 assay indicating the proliferation of CDSCs in collagen hydrogels with different concentrations of PR1P. (B, C) ZsGreen fluorescence intensity of CDSCs in composite hydrogels and detailed statistics. Scale bar: 500 μm (4x) and 200 μm (10x). (D, E) FAK staining of CDSCs treated with collagen hydrogel containing various doses of PR1P. Scale bar: 200 μm. $^{*}p < 0.05$, $^{**}p < 0.01$ compared as denoted by bar. Values are expressed as means ± SD.

Meanwhile, we did not observe obvious pathological changes in the heart, liver, and kidney structures of the animals that underwent gel transplantation (Fig. 11F).

Overall, these results indicate that the transplantation of CDSC-laden PR1P collagen hydrogel not only enhances new bone formation and the regeneration of new blood vessels but also suppresses osteoclastogenesis, thereby promoting comprehensive bone defect healing.

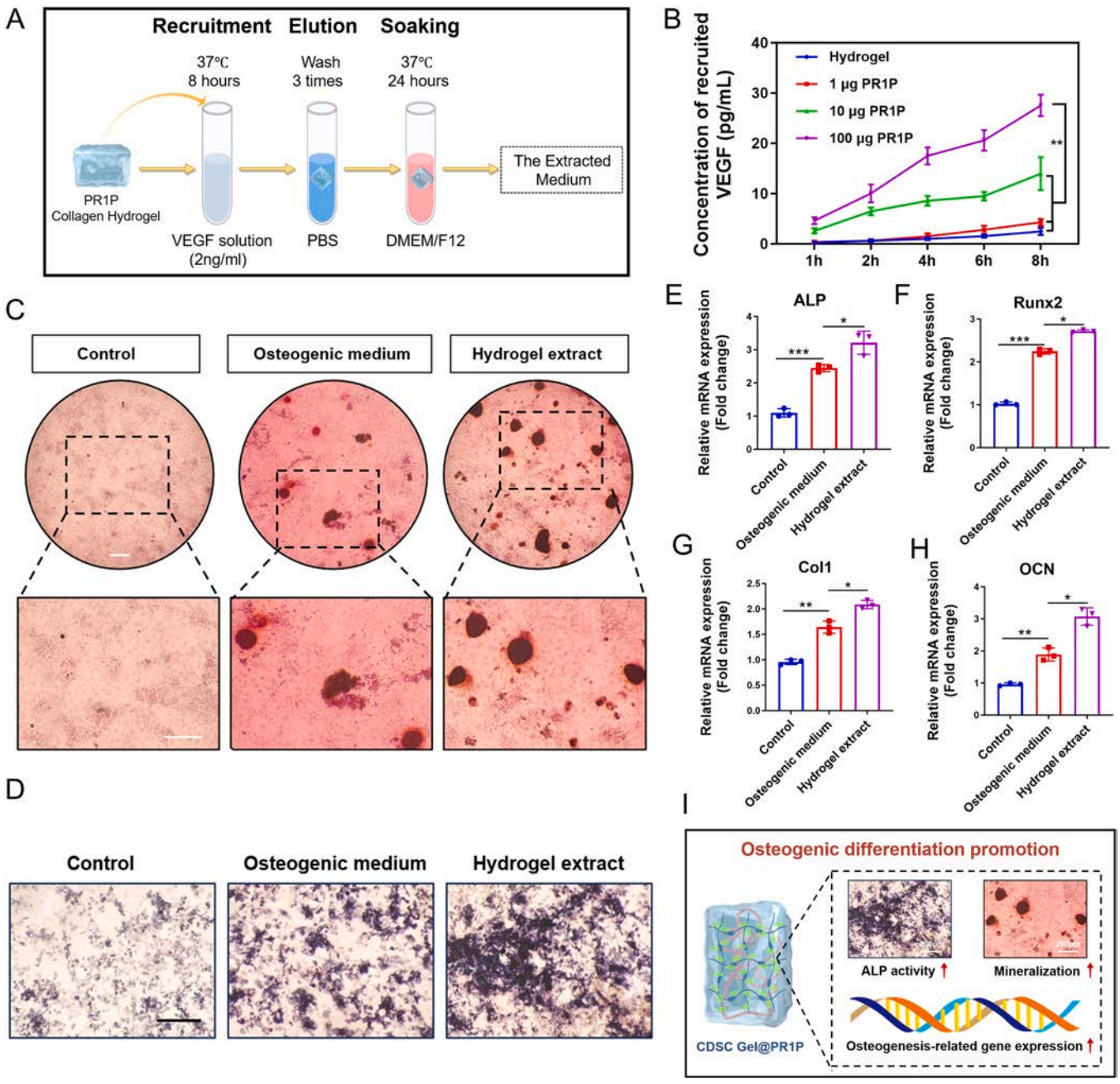

Fig. 4. The VEGF recruitment ability of composite hydrogels and its effect on osteogenic differentiation of CDSCs in vitro. (A) Schematic diagram of VEGF recruitment experiment in vitro. (B) ELISA assay indicating the VEGF recruitment ability of collagen hydrogels with different concentrations of PR1P. (C—H) ALP staining, ARS staining, and expression level of osteogenic marker genes indicating the effect of composite hydrogels on CDSCs osteogenic differentiation. Scale bar: 200 μm. (I) Osteogenic differentiation-promoting effect of composite hydrogels on CDSCs. *$p < 0.05$, **$p < 0.01$, ***$p < 0.001$, ****$p < 0.0001$ compared as denoted by bar. Values are expressed as means ± SD.

4. Discussion

Bone defect repair presents a significant challenge for clinicians, with autogenous bone grafting remaining the gold standard, particularly for critical-sized defects [45]. The development of bone tissue engineering approaches offers promising alternatives, yet identifying appropriate seed cells is a key priority in this field [46,47]. BMSCs and ADSCs have demonstrated potential for bone regeneration, but their clinical application is hindered by limited availability, inadequate proliferation, and low survival rates [48]. Ideal seed cells should possess strong osteogenic activity, be readily available, and adapt well to the hypoxic, nutrient-deficient conditions encountered post-transplantation.

Costal cartilage, the richest cartilage tissue in the human body, has gained recent popularity in plastic surgery due to its simple structure, ease of purification, and availability [49]. Notably, incidences of primary or secondary tumors associated with costal cartilage, including post-transplantation cases, are exceedingly rare [20,21]. Previous research successfully isolated CDSCs, confirming their proliferation ability and multilineage differentiation potential. CDSCs not only survive and proliferate but also gradually regenerate BTI structures in situ following transplantation, indicating their suitability as seed cells for tissue-engineered regeneration [22]. The current research further supports the hypothesis that CDSCs hold significant potential for bone

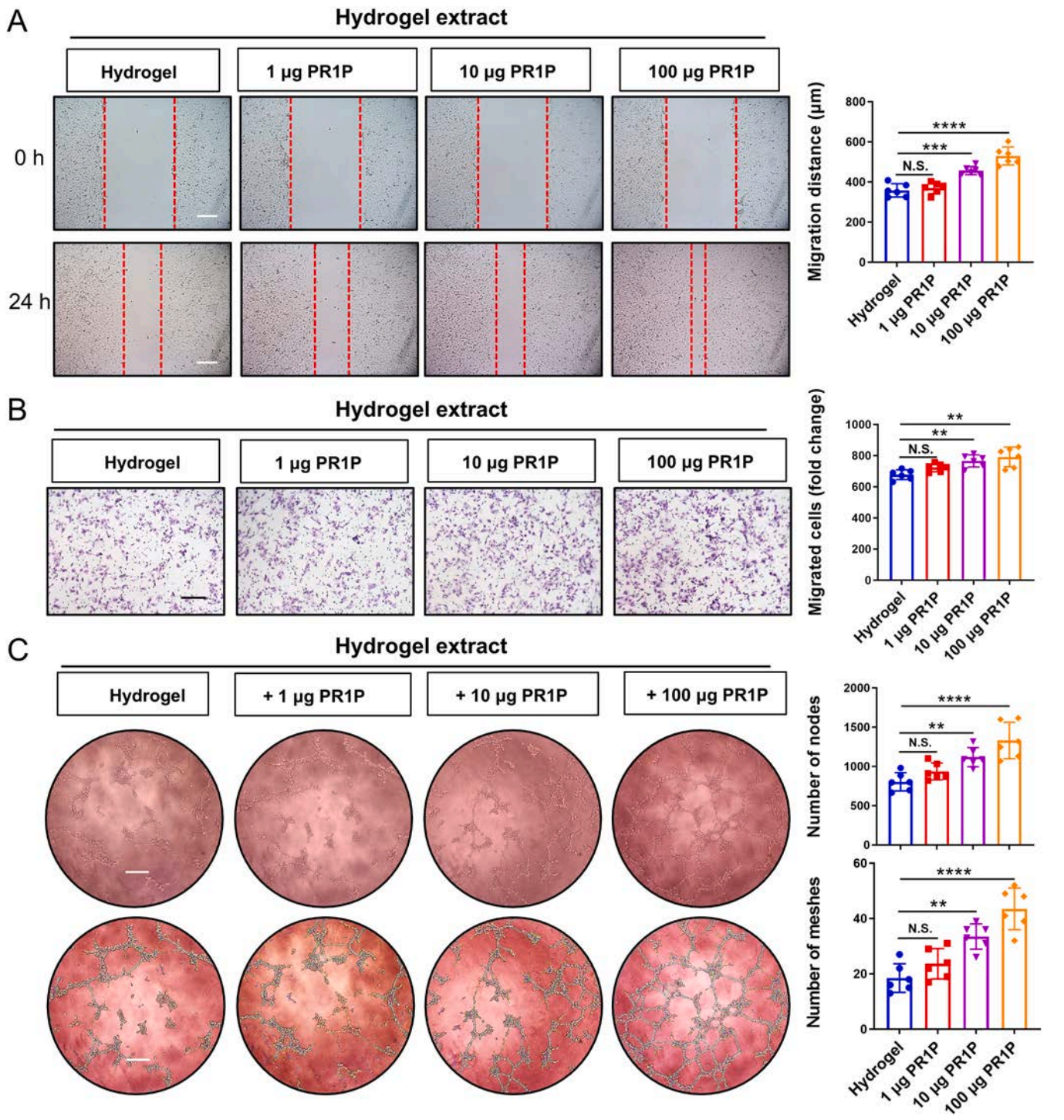

Fig. 5. Effect of composite hydrogels on HUVEC migration and endothelial network assembly in vitro. (A) Scratch wound healing assay of HUVECs treated with composite hydrogels and corresponding statistical results. (B) Transwell assay of HUVECs treated with composite hydrogels and corresponding statistical results. (C) Tube formation assay of HUVECs treated with composite hydrogels and corresponding statistical results. Scale bar: 200 μm. $^{*}p < 0.05$, $^{**}p < 0.01$, $^{***}p < 0.001$ compared as denoted by bar. Values are expressed as means ± SD.

defect repair, as they demonstrated the ability to thrive in the low-oxygen and low-nutrient environments typical of bone defects, maintaining long-term viability post-transplantation while differentiating into osteogenic lineages, thereby facilitating in situ bone tissue regeneration.

Angiogenesis plays a critical role in bone regeneration, with VEGF being a key factor in inducing vascularization [24]. However, VEGF's large molecular size and short half-life limit its effectiveness in biomaterials [28].

To address this, a 12-amino acid peptide (PR1P) containing three conserved β-sheet forming residues was introduced. PR1P can be slowly released from the hydrogel in the local microenvironment, facilitating endogenous VEGF recruitment to promote early-stage angiogenesis at the defect site.

The incorporation of VEGF-recruiting PR1P into the composite hydrogel significantly enhanced both angiogenesis and osteogenic

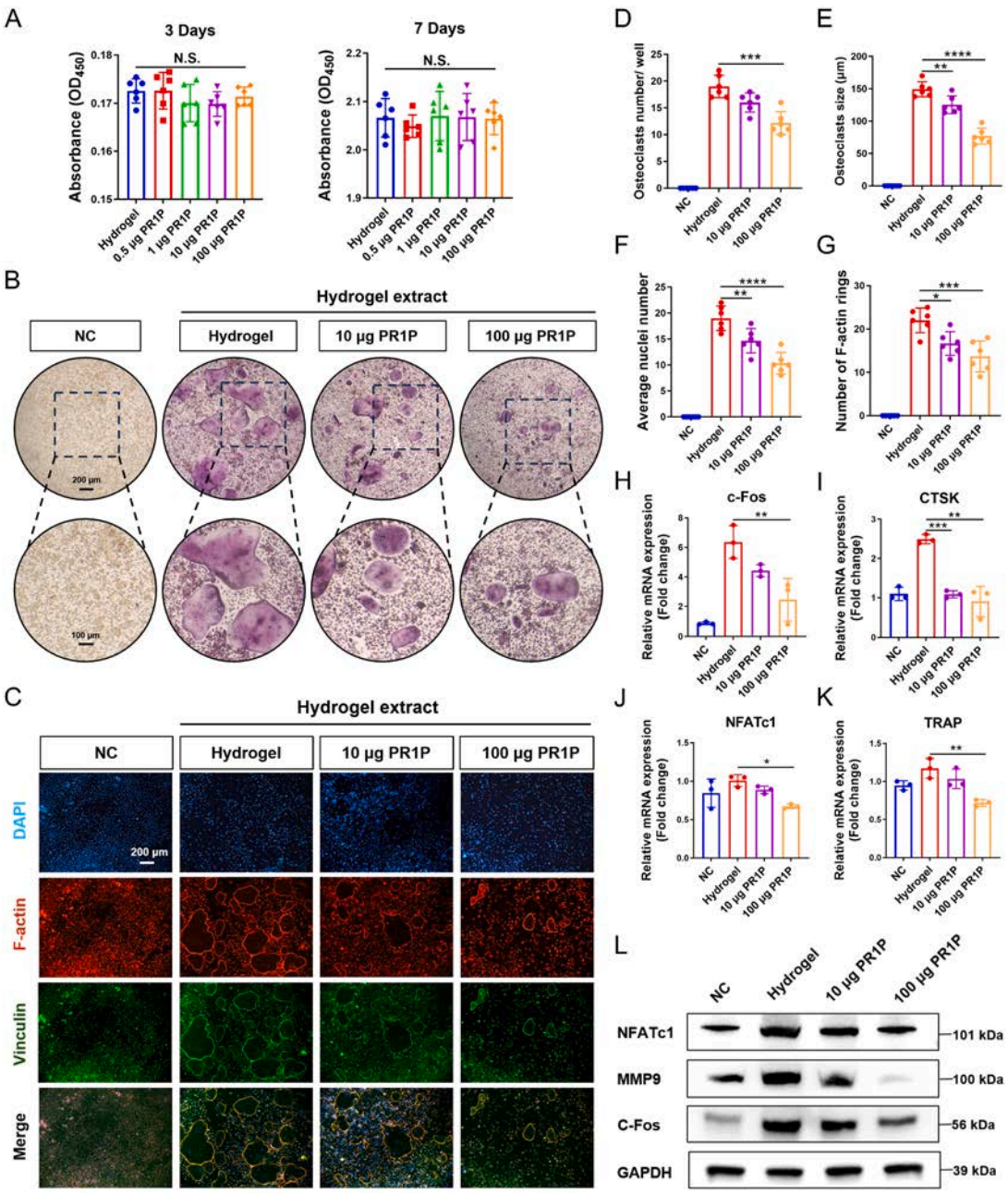

Fig. 6. Effect of composite hydrogels on osteoclastogenesis in vitro. (A) RANKL-induced BMMs were exposed to PR1P-incorporated hydrogel extracts at gradient concentrations for 3 and 7 days, followed by CCK-8 viability assessment to quantify cytocompatibility. (B-G) TRAP and FAK staining demonstrated the pharmacological attenuation of osteoclastogenesis by PR1P-incorporated hydrogel extracts. (H-K) The effect of PR1P collagen hydrogel on the expression of osteoclast-specific genes (CTSK, MMP9, NFATc1, and c-Fos) was quantitatively assessed by qRT-PCR. (L) Western blot analysis of osteoclast markers during osteoclastogenesis following PR1P collagen hydrogel treatment. Scale bar: 200 μm. $^{*}p < 0.05$, $^{**}p < 0.01$, $^{***}p < 0.001$ compared as denoted by bar. Values are expressed as means ± SD.

differentiation of CDSCs, ultimately accelerating the healing of bone defects.

Collagen hydrogels are widely used in tissue engineering as scaffolding materials due to their good biocompatibility and availability [50]. In this study, collagen hydrogel was successfully extracted from rat tail tendon and utilized as a biological scaffold for loading seed cells and bioactive factors, further underscoring its potential for bone tissue engineering.

The schematic diagram of CDSC-laden PR1P collagen hydrogel preparation and the mechanism of promoting bone defect repair are shown in Fig. 1. Comprehensive characterization of the hydrogel revealed a porous, honeycomb-like structure, which facilitates an optimal microenvironment for stem cell proliferation and differentiation by enhancing nutrient transport and waste removal. Additionally, the hydrogel demonstrated rapid gelation and slow in vivo degradation, ensuring the long-term survival of CDSCs post-transplantation. Release studies indicated that PR1P can be gradually released in the local microenvironment, a key factor for the efficient recruitment of VEGF and subsequent vascular growth at the bone defect site. However, it is necessary to further enhance the mechanical stability of the hydrogel in the follow-up research.

To further assess the key components of the CDSC-laden PR1P collagen hydrogel and their effectiveness as biological scaffolds for bone repair, a combination of non-targeted metabolomics and network

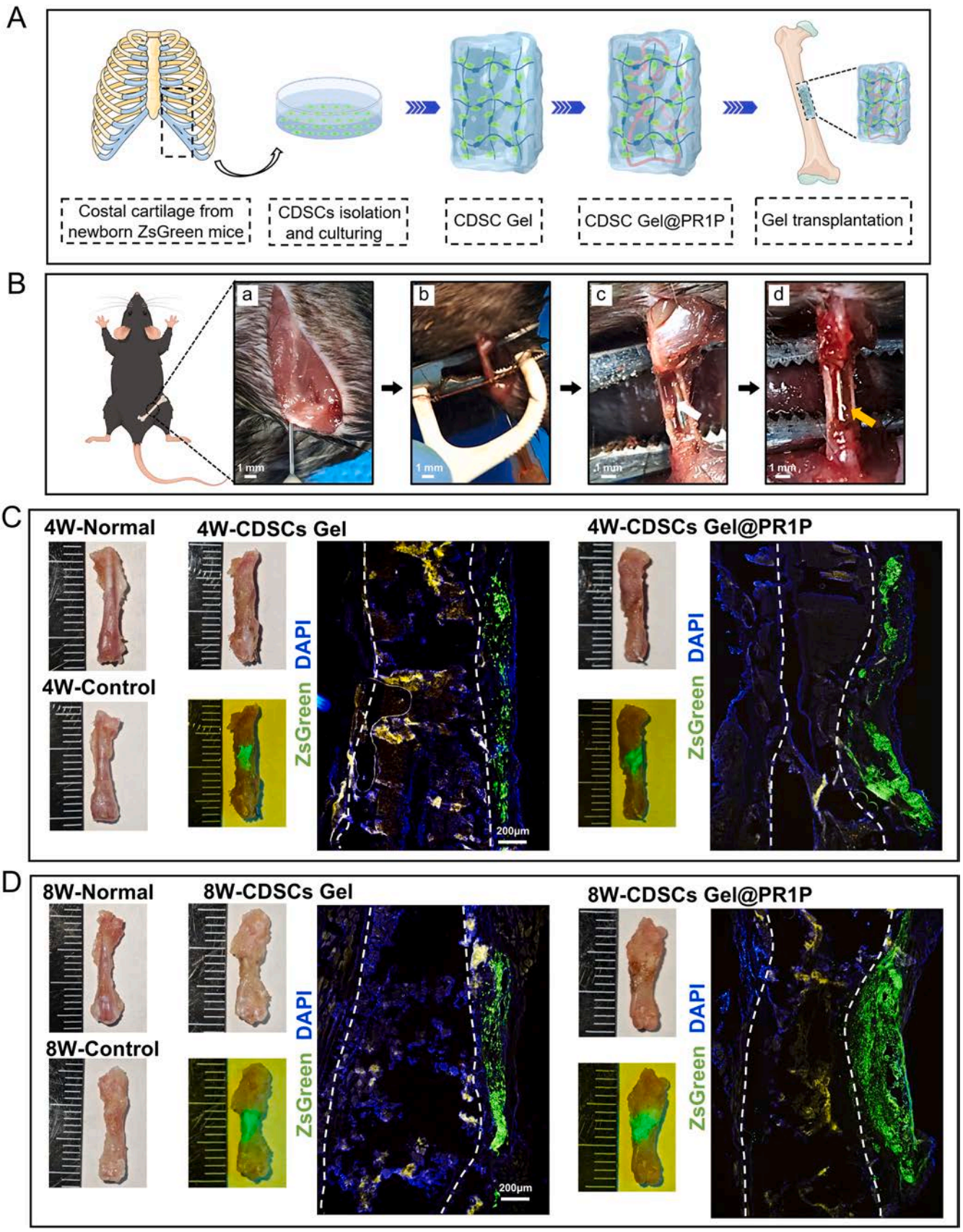

Fig. 7. In vivo bone repair assessment of CDSC-laden PR1P collagen hydrogels. (A) The workflow of the animal experiment. (B) The detailed surgical procedure of the femoral defect model in mice. (C) The gross appearance of the femurs and the ZsGreeen fluorescence of CDSCs at 4 weeks after composite hydrogels transplantation. (D) The gross appearance of the femurs and the ZsGreeen fluorescence of CDSCs at 8 weeks after composite hydrogels transplantation. White dashed line: boundary between bone marrow (BM) and newly formed bone (NFB). Scale bar: 500 μm.

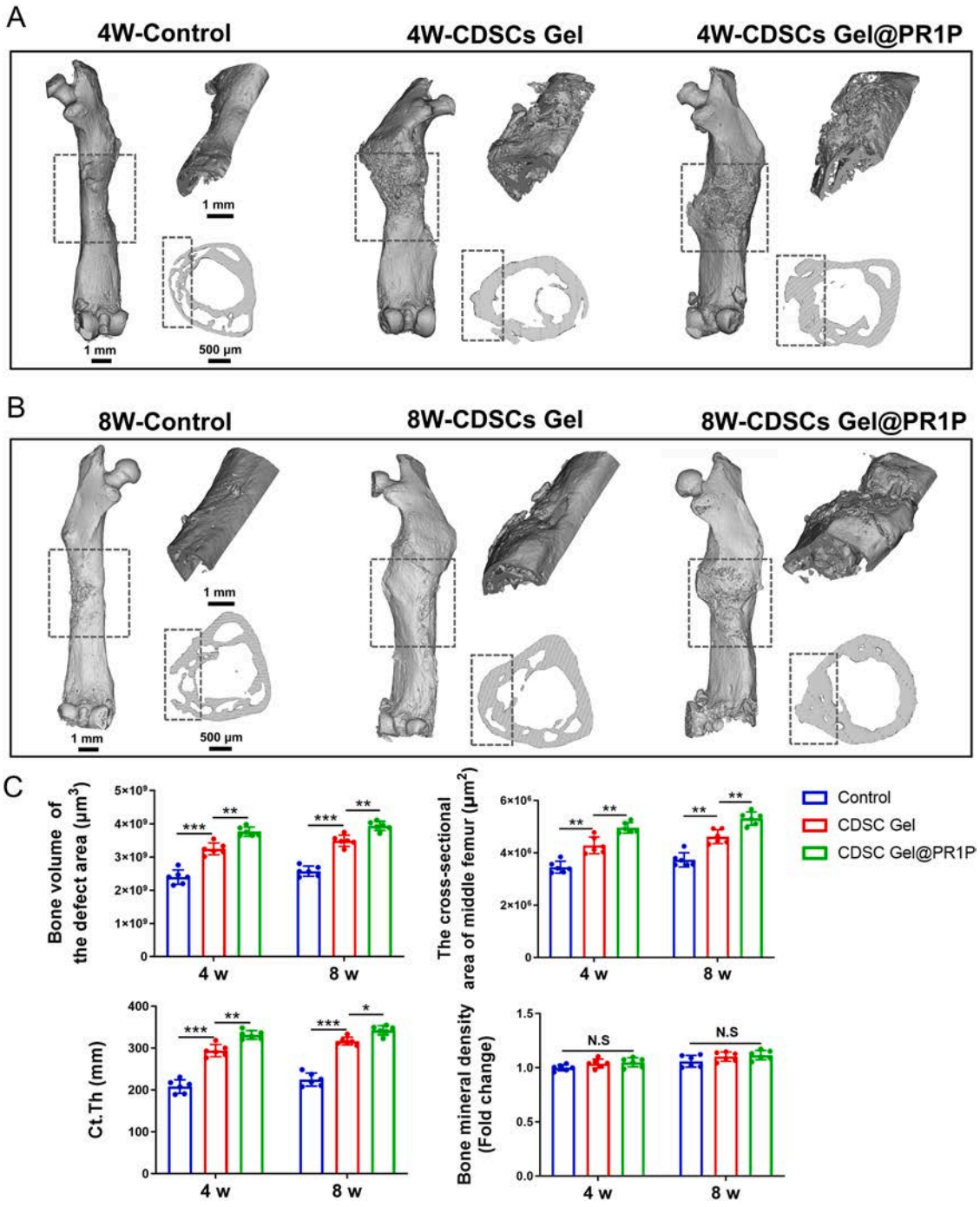

Fig. 8. Reconstructed 3D micro-CT analysis at 4 and 8 weeks after transplantation of CDSC-laden PR1P collagen hydrogels in femur defect model. (A) Micro-CT images at 4 weeks after transplantation of hydrogels. (B) Micro-CT images at 8 weeks after transplantation of hydrogels. (C) Quantification of bone volume of the defect area, cross-sectional area of middle femur, Ct. Th, and BMD. $^{*}p < 0.05$, $^{**}p < 0.01$, $^{***}p < 0.001$ compared as denoted by bar. Values are expressed as means ± SD ($n = 6$).

pharmacology analyses was employed. Network pharmacology results revealed that the potential target genes of the hydrogel's primary metabolic components were highly associated with bone regeneration. Gene enrichment analyses reinforced the hydrogel's suitability for promoting cell proliferation and angiogenesis.

Beyond its structural benefits, the hydrogel displayed favorable biocompatibility and efficacy in enhancing the osteogenic differentiation of CDSCs. Notably, CDSCs cultured within the hydrogel exhibited robust proliferative activity and upregulated expression of key osteogenic markers, including RUNX2, OCN, and COL1A1.

Previous studies have already established VEGF's critical role in osteogenesis [51]. In line with this, the VEGF-recruiting PR1P collagen hydrogel significantly boosted ALP activity and calcium deposition in CDSCs, both of which are critical indicators of osteogenic differentiation [52]. The angiogenic potential of the PR1P collagen hydrogel via VEGF recruitment was further validated in vitro. The results demonstrated that the VEGF-recruited PR1P hydrogel effectively enhanced HUVEC proliferation, migration, and assembly into cord-like networks, confirming its potential to promote key initiating steps of angiogenesis. In addition, osteoclasts serve as critical regulators of bone homeostasis. Our study

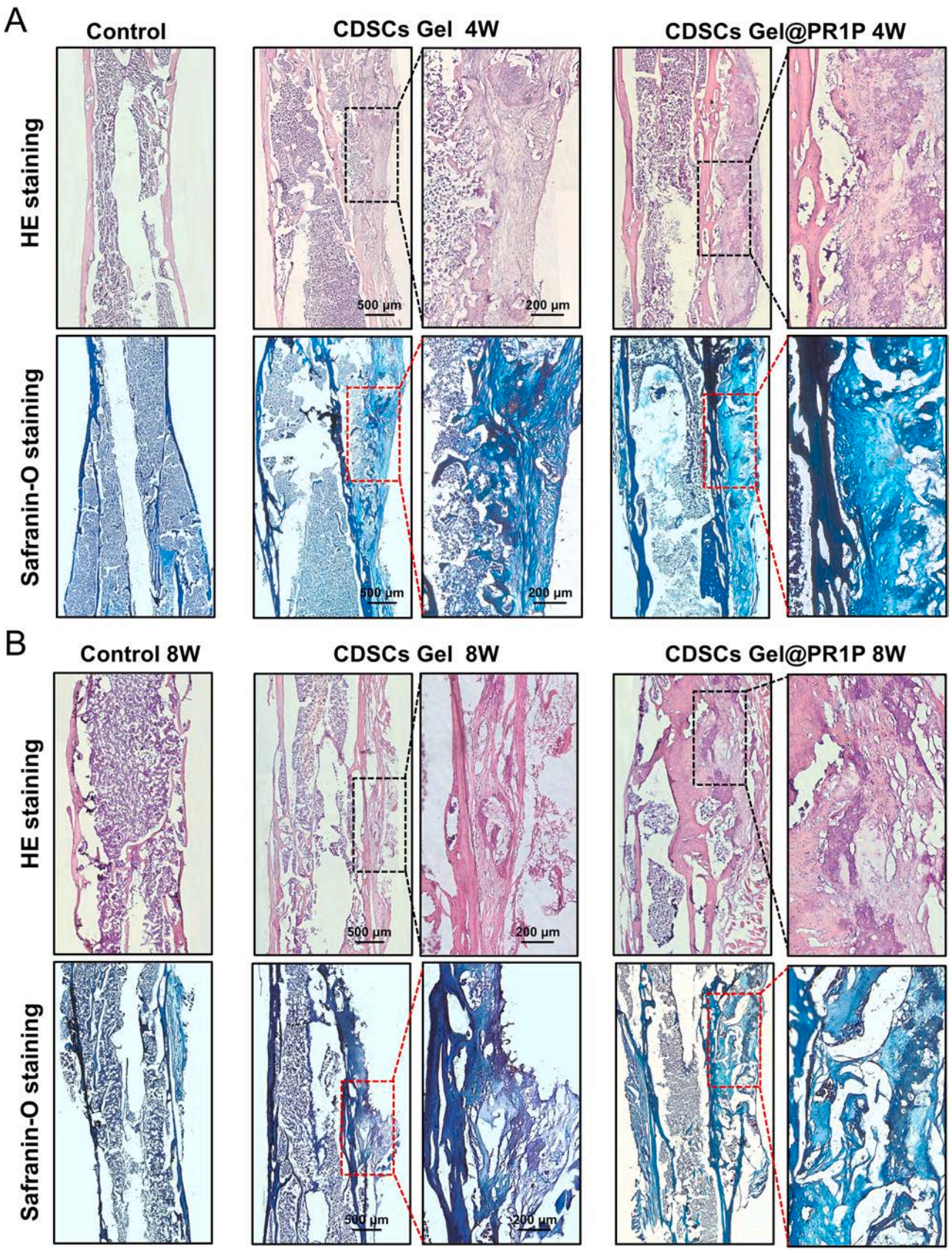

Fig. 9. Histological analysis after transplantation of CDSC-laden PR1P collagen hydrogels in femur defect model. (A) The H&E and S-O staining results at 4 weeks after transplantation of hydrogels. (B) The H&E and S-O staining results at 8 weeks after transplantation of hydrogels. Scale bar: 500 μm (200 μm in magnified view).

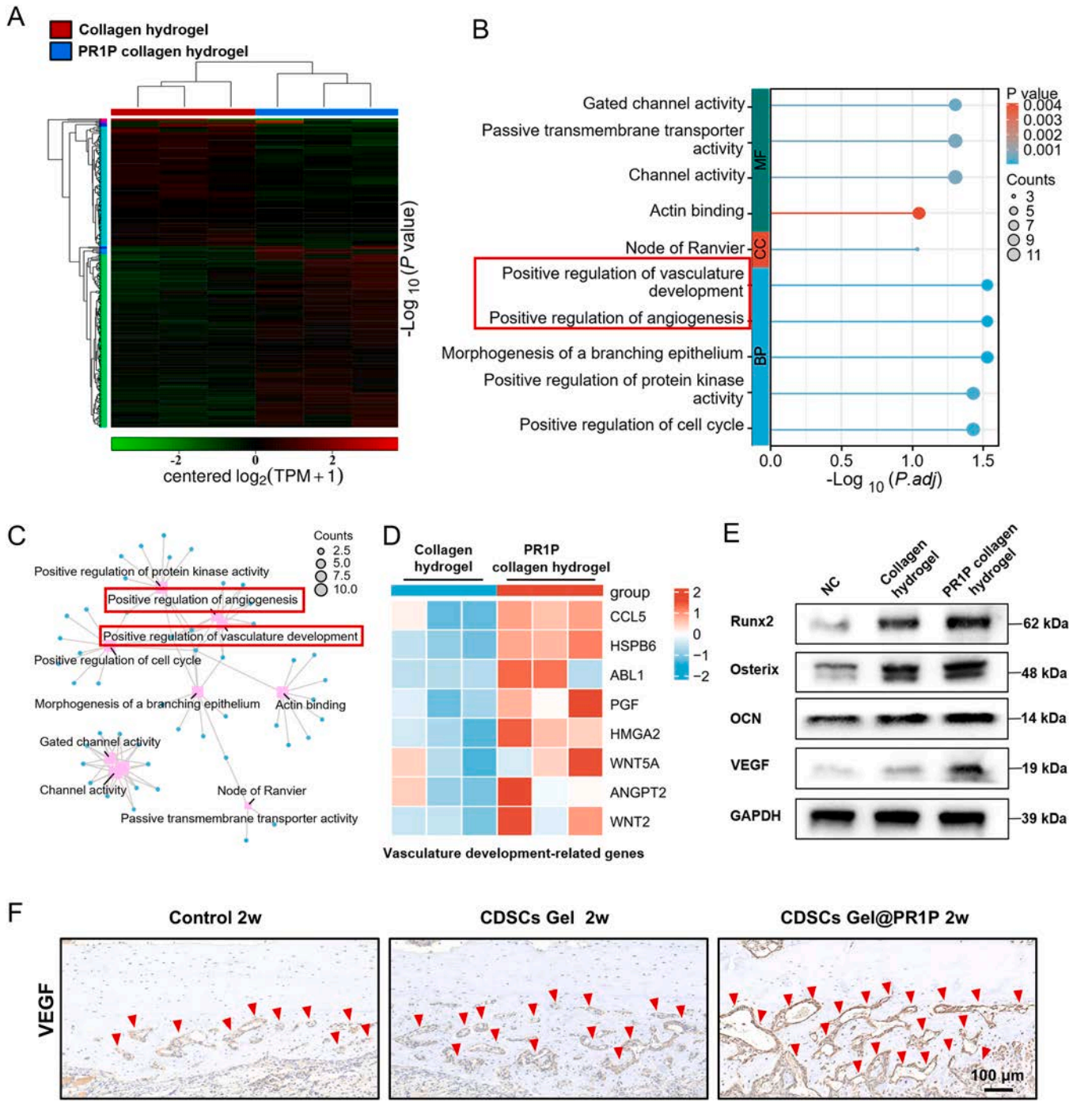

Fig. 10. PR1P collagen hydrogel enhances CDSCs osteogenic differentiation through VEGF signaling. (A) Heatmap of clustering analysis. (B, C) GO enrichment analysis of PR1P collagen hydrogel group VS collagen hydrogel. (D) Heatmap illustrating the high expression of vasculature development-related genes in the PR1P collagen hydrogel group via transcriptome analysis. (E) Western blot results show that PR1P collagen hydrogel promotes osteogenic differentiation of CDSCs through the VEGF signaling. (F) IHC staining of VEGF in femur defect model.

revealed that PR1P collagen gel exhibits a marked inhibitory effect on osteoclast differentiation in vitro.

Finally, these findings were corroborated in vivo using a femur defect model. Femurs were harvested at 4 and 8 weeks post-transplantation, revealing stable ZsGreen fluorescence throughout the defect area. This indicated the sustained survival and proliferation capacity of CDSCs within the post-transplantation microenvironment, aligning with previous research. Micro-CT is a crucial technique for assessing bone defect repair, and the results in this study showed that the CDSC transplantation groups exhibited more newly formed bone, larger cross-sectional area of the mid-femur, and increased cortical bone thickness compared to the control group. Among these, the CDSCs gel@PR1P group demonstrated the most effective bone repair. H&E and S-O staining further confirmed superior repair outcomes in the CDSCs transplantation groups, as evidenced by increased new bone formation and thicker cortical bone. Endochondral osteogenesis is pivotal in the repair and remodeling of long bone defects [53]. In this study, although some chondrocyte-like cells remained in the outer layer of the femur in the CDSCs transplantation groups, hard callus (woven bone) had gradually formed and replaced the cartilage through endochondral

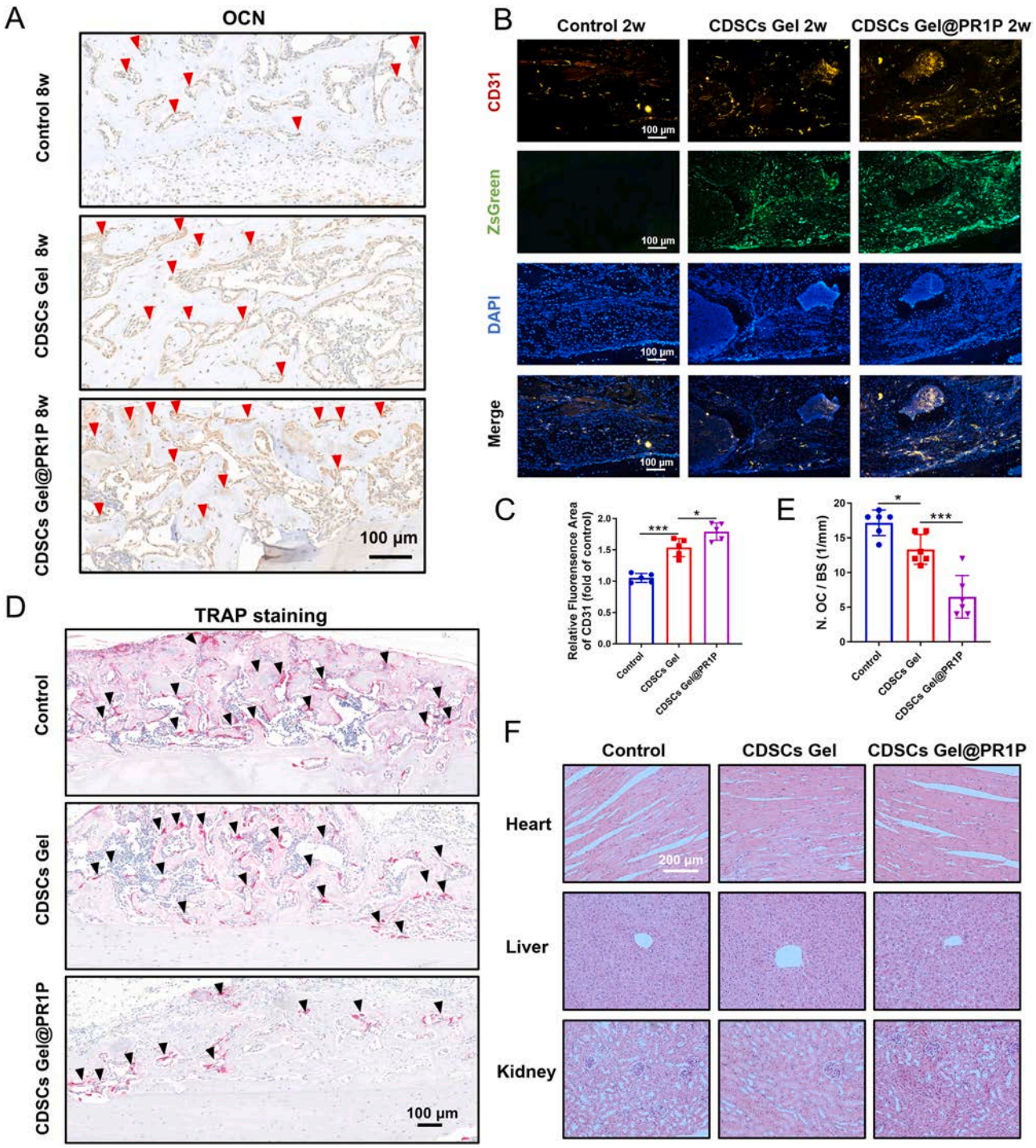

Fig. 11. CDSC-laden PR1P collagen hydrogel promotes osteogenesis and angiogenesis and inhibits osteoclastogenesis in vivo. (A) IHC staining of OCN in femur defect model at 8 weeks after transplantation of hydrogels. Scale bar: 100 μm. (B, C) The immunofluorescence staining of CD31 on representative sections of femurs at 4 weeks after transplantation of hydrogels and quantitative analysis. Scale bar: 100 μm. (D, E) Representative images of TRAP staining in femur defect model at 8 weeks after hydrogel transplantation and quantitative analysis. Scale bar: 100 μm. (F) Pathological changes in the heart, liver, and kidney structures of the animals. $^{*}p < 0.05$, $^{**}p < 0.01$ compared as denoted by bar. Values are expressed as means ± SD.

ossification from the outside to the inside. In the innermost layer, the transplanted CDSCs differentiated sufficiently to form mature cortical bone. The IHC analysis of OCN further substantiated the pro-osteogenic effect of CDSC-laden PR1P collagen hydrogel on osseous regeneration at bone defect grafting sites.

Furthermore, to investigate the underlying mechanisms by which the composite hydrogel promotes CDSCs osteogenic differentiation, we performed transcriptome sequencing analysis. GO enrichment results of DEGs revealed significant enrichment in biological processes related to vasculature development. Transcriptomic profiling of angiogenesis-associated genes consistently supported these findings, suggesting that the pro-osteogenic effects of the composite hydrogel might be mediated through VEGF signaling pathway. Subsequent validation experiments employing western blot analysis and in vivo immunohistochemical staining corroborated these conclusions.

The CDSCs gel@PR1P group, benefiting from in situ VEGF

recruitment, exhibited enhanced angiogenesis in the local bone defect microenvironment, reflected by the strongest CD31 fluorescence, a marker of vascular endothelium. Rapid and sufficient angiogenesis is essential for effective bone defect healing [54]. In this group, PR1P released from the composite hydrogel recruited significant amounts of endogenous VEGF to the bone defect site, facilitating angiogenesis and creating a more favorable osteogenic environment compared to the CDSCs gel group.

TRAP, an established marker of mature osteoclasts, is routinely employed to trace the differentiation commitment of osteoclast precursors [55]. TRAP staining at femoral defect sites with hydrogel implantation in murine models revealed that CDSC-laden PR1P collagen hydrogel exerted a potent inhibitory effect on osteoclastogenesis. Plausible mechanistic underpinnings for this effect may involve multi-dimensional regulatory layers: (1) RANKL/OPG axis modulation—PR1P may skew the RANKL/OPG balance via OPG upregulation or RANKL downregulation in the defect niche; (2) NF-κB signaling interference—PR1P could dampen NF-κB activation to attenuate RANKL-driven osteoclast differentiation; (3) Angiogenesis-osteogenesis crosstalk—PR1P-enhanced angiogenesis remodels the microenvironment (e.g., oxygen/cytokine profiles) to indirectly suppress osteoclasts [35,56]. Further works are still waiting to be improved and completed.

In summary, the findings indicate that CDSCs serve as suitable seed cells for bone tissue engineering. The CDSC-laden PR1P collagen hydrogel, with its function of promoting angiogenesis and osteogenesis and inhibiting osteoclastogenesis, demonstrates favorable potential as a biomaterial for bone defect repair and regeneration.

However, several limitations exist in this study. First, the in vivo mechanisms underlying the osteogenic differentiation of CDSCs have not been fully explored. Our research group is addressing this through studies involving gene editing in mice and single-cell sequencing technologies. Additionally, the bone regeneration potential of CDSCs at various developmental stages needs to be evaluated. Further research is necessary to determine whether the osteogenic differentiation capacity of CDSCs is innate or acquired through in vitro cultivation. An inherent limitation lies in the lack of a collagen hydrogel + PR1P group without CDSCs transplantation, which impedes independent evaluation of PR1P's role in host cell recruitment, VEGF-mediated angiogenesis, and bone repair, as well as the synergistic crosstalk between CDSCs and PR1P. Furthermore, although functional outcomes and prior mechanistic evidence support the VEGF recruitment hypothesis, direct dynamic quantification of VEGF levels at the bone defect site remains technically challenging. Future investigations employing intravital imaging (e.g., VEGF-A reporter mouse models) or microdialysis would help conclusively elucidate the spatiotemporal dynamics of PR1P-mediated VEGF recruitment during bone regeneration. Finally, recent advancements in photothermal therapy have demonstrated its potential to synergistically enhance bone repair by modulating immune responses, scavenging reactive oxygen species (ROS), and promoting angiogenesis [57,58]. Coupling photothermal therapy with stem cell-driven osteogenesis (e.g., CDSC differentiation) may offer a promising strategy to further optimize bone regeneration in complex microenvironments.

5. Conclusion

This study is the first to show the potential of CDSCs as viable seed cells for bone tissue engineering. A CDSC-laden PR1P collagen hydrogel was developed, which effectively recruits endogenous VEGF, facilitating angiogenesis and creating an optimal osteogenic microenvironment. Additionally, the inhibitory effect of the composite hydrogel on osteoclastogenesis also contributes to bone repair. In vivo transplantation of this composite hydrogel significantly enhanced femoral defect healing in mice by promoting both bone formation and vascular regeneration and suppressing osteoclastogenesis. Overall, the findings present a promising strategy for bone defect repair, highlighting the strong potential of the CDSCs-based bone tissue engineering approach for future clinical applications.

Data availability

Data will be made available on request.

CRediT authorship contribution statement

Chenhui Cai: Writing – review & editing, Writing – original draft, Software, Methodology, Conceptualization. **Rui Zuo:** Software, Formal analysis, Conceptualization. **Zaoqing Zhang:** Formal analysis. **Haoke Li:** Methodology. **Zhongyi Liu:** Methodology. **Xu Zhao:** Software. **Mohamed EL-Newehy:** Methodology. **Meera Moydeen Abdulhameed:** Methodology. **Zhengchao Yuan:** Supervision, Methodology, Conceptualization. **Xiumei Mo:** Supervision, Methodology, Conceptualization. **Tongwei Chu:** Writing – review & editing, Supervision, Funding acquisition. **Chao Zhang:** Writing – review & editing, Supervision, Funding acquisition, Conceptualization.

Declaration of competing interest

The authors declare that they have no known competing financial interests or personal relationships that could have appeared to influence the work reported in this paper.

Acknowledgment

We thank the picture materials by Figdraw (www.figdraw.com). We thank Bullet Edits Limited for the linguistic editing and proofreading of the manuscript. We thank Home for Researchers (www.home-for-researchers.com) for their assistance with the mechanism diagrams in this manuscript. This work was supported by the Major Program of the National Natural Science Foundation of China (Grant No 82192884), Young and Middle-aged Medical High-end Talent Project of Chongqing (Grant No YXGD202401), Key Project of Chongqing Technology Innovation and Application Development Special Project (Grant No CSTB2022TIAD-KPX0192), Graduate Student Scientific Research Innovation Projects of Chongqing (Grant No CYB23290) and Science and Technology Commission of Shanghai Municipality, China (20DZ2254900). This project was also supported by Ongoing Research Funding program (ORF-2025-769), King Saud University, Riyadh, Saudi Arabia.

Supplementary materials

Supplementary material associated with this article can be found, in the online version, at doi:10.1016/j.actbio.2025.07.023.

References

[1] R. Dimitriou, E. Jones, D. McGonagle, P.V. Giannoudis, Bone regeneration: current concepts and future directions, BMC. Med. 9 (2011) 66, https://doi.org/10.1186/1741-7015-9-66.
[2] Y. He, F. Li, P. Jiang, F. Cai, Q. Lin, M. Zhou, H. Liu, F. Yan, Remote control of the recruitment and capture of endogenous stem cells by ultrasound for in situ repair of bone defects, Bioact. Mater. 21 (2023) 223–238, https://doi.org/10.1016/j.bioactmat.2022.08.012.
[3] Y. Huang, L. Zhang, Y. Ji, H. Deng, M. Long, S. Ge, Y. Su, S.Y. Chan, X.J. Loh, A. Zhuang, J. Ruan, A non-invasive smart scaffold for bone repair and monitoring, Bioact. Mater. 19 (2023) 499–510, https://doi.org/10.1016/j.bioactmat.2022.04.034.
[4] Q. Yao, J.G. Cosme, T. Xu, J.M. Miszuk, P.H. Picciani, H. Fong, H. Sun, Three dimensional electrospun PCL/PLA blend nanofibrous scaffolds with significantly improved stem cells osteogenic differentiation and cranial bone formation, Biomaterials 115 (2017) 115–127, https://doi.org/10.1016/j.biomaterials.2016.11.018.
[5] R. Agarwal, A.J. García, Biomaterial strategies for engineering implants for enhanced osseointegration and bone repair, Adv. Drug Deliv. Rev. 94 (2015) 53–62, https://doi.org/10.1016/j.addr.2015.03.013.

[6] K.A. White, R.M. Olabisi, Spatiotemporal control strategies for bone formation through tissue engineering and regenerative medicine approaches, Adv. Healthc. Mater. 8 (2) (2019) e1801044, https://doi.org/10.1002/adhm.201801044.
[7] R. Guo, H. Zhuang, X. Chen, Y. Ben, M. Fan, Y. Wang, P. Zheng, Tissue engineering in growth plate cartilage regeneration: mechanisms to therapeutic strategies, J. Tissue Eng. 14 (2023) 20417314231187956, https://doi.org/10.1177/20417314231187956.
[8] Z. Hao, H. Li, Y. Wang, Y. Hu, T. Chen, S. Zhang, X. Guo, L. Cai, J. Li, Supramolecular Peptide Nanofiber Hydrogels for Bone Tissue Engineering: From Multihierarchical Fabrications to Comprehensive Applications, Advanced science, 9, Weinheim, Baden-Wurttemberg, Germany, 2022 e2103820, https://doi.org/10.1002/advs.202103820.
[9] S. Chen, X. Chen, Z. Geng, J. Su, The horizon of bone organoid: a perspective on construction and application, Bioact. Mater. 18 (2022) 15–25, https://doi.org/10.1016/j.bioactmat.2022.01.048.
[10] M. Zhang, J.P. Matinlinna, J.K.H. Tsoi, W. Liu, X. Cui, W.W. Lu, H. Pan, Recent developments in biomaterials for long-bone segmental defect reconstruction: a narrative overview, J. Orthop. Translat. 22 (2020) 26–33, https://doi.org/10.1016/j.jot.2019.09.005.
[11] S.R. Park, J.W. Kim, H.S. Jun, J.Y. Roh, H.Y. Lee, I.S. Hong, Stem cell secretome and its effect on cellular mechanisms relevant to wound healing, Molecular therapy: the journal of the American Society of Gene Therapy 26 (2) (2018) 606–617, https://doi.org/10.1016/j.ymthe.2017.09.023.
[12] P. Bora, A.S. Majumdar, Adipose tissue-derived stromal vascular fraction in regenerative medicine: a brief review on biology and translation, Stem Cell Res. Ther. 8 (1) (2017) 145, https://doi.org/10.1186/s13287-017-0598-y.
[13] S. Park, K.A. Rahaman, Y.C. Kim, H. Jeon, H.S. Han, Fostering tissue engineering and regenerative medicine to treat musculoskeletal disorders in bone and muscle, Bioact. Mater. 40 (2024) 345–365, https://doi.org/10.1016/j.bioactmat.2024.06.022.
[14] C.K.F. Chan, G.S. Gulati, R. Sinha, J.V. Tompkins, M. Lopez, A.C. Carter, R. C. Ransom, A. Reinisch, T. Wearda, M. Murphy, R.E. Brewer, L.S. Koepke, O. Marecic, A. Manjunath, E.Y. Seo, T. Leavitt, W.J. Lu, A. Nguyen, S.D. Conley, A. Salhotra, T.H. Ambrosi, M.R. Borrelli, T. Siebel, K. Chan, K. Schallmoser, J. Seita, D. Sahoo, H. Goodnough, J. Bishop, M. Gardner, R. Majeti, D.C. Wan, S. Goodman, I.L. Weissman, H.Y. Chang, M.T. Longaker, Identification of the Human skeletal stem cell, Cell 175 (1) (2018) 43–56, https://doi.org/10.1016/j.cell.2018.07.029, e21.
[15] M.P. Murphy, L.S. Koepke, M.T. Lopez, X. Tong, T.H. Ambrosi, G.S. Gulati, O. Marecic, Y. Wang, R.C. Ransom, M.Y. Hoover, H. Steininger, L. Zhao, M. P. Walkiewicz, N. Quarto, B. Levi, D.C. Wan, I.L. Weissman, S.B. Goodman, F. Yang, M.T. Longaker, C.K.F. Chan, Articular cartilage regeneration by activated skeletal stem cells, Nat. Med. 26 (10) (2020) 1583–1592, https://doi.org/10.1038/s41591-020-1013-2.
[16] S.R. Singh, W. Liu, S.X. Hou, The adult Drosophila malpighian tubules are maintained by multipotent stem cells, Cell Stem Cell 1 (2) (2007) 191–203, https://doi.org/10.1016/j.stem.2007.07.003.
[17] J.C. Lui, M. Colbert, C.S.F. Cheung, M. Ad, A. Lee, Z. Zhu, K.M. Barnes, D. S. Dimitrov, J. Baron, Cartilage-targeted IGF-1 treatment to promote longitudinal bone growth, Molecular therapy: the journal of the American Society of Gene Therapy 27 (3) (2019) 673–680, https://doi.org/10.1016/j.ymthe.2019.01.017.
[18] Y. Gao, J. Gao, H. Li, D. Du, D. Jin, M. Zheng, C. Zhang, Autologous costal chondral transplantation and costa-derived chondrocyte implantation: emerging surgical techniques, Ther. Adv. Musculoskelet. Dis. 11 (2019), https://doi.org/10.1177/1759720x19877131, 1759720x19877131.
[19] S.H. Yoo, Y.J. Jang, Rib cartilage in Asian rhinoplasty: new trends, current opinion in otolaryngology & head and neck surgery 27(4) (2019) 261–266. https://doi.org/10.1097/moo.0000000000000547.
[20] R.H. Wallace, J.R. Lingley, Chondroma of eighth costal cartilage, N. Engl. J. Med. 235 (18) (1946) 663–665.
[21] N. Zy, [Giant chondroma of the costal cartilages], Khirurgiia (Mosk) (11) (1982) 93–94.
[22] R. Zuo, J. Liu, Y. Zhang, H. Zhang, J. Li, J. Wu, Y. Ji, S. Mao, C. Li, Y. Zhou, Y. Wu, D. Cai, Y. Sun, C. Zhang, In situ regeneration of bone-to-tendon structures: comparisons between costal-cartilage derived stem cells and BMSCs in the rat model, Acta Biomater. 145 (2022) 62–76, https://doi.org/10.1016/j.actbio.2022.03.056.
[23] Y. Peng, S. Wu, Y. Li, J.L. Crane, Type H blood vessels in bone modeling and remodeling, Theranostics. 10 (1) (2020) 426–436, https://doi.org/10.7150/thno.34126.
[24] H.S. Kim, H.S. Ha, D.H. Kim, D.H. Son, S. Baek, J. Park, C.H. Lee, S. Park, H. J. Yoon, S.E. Yu, J.I. Kang, K.M. Park, Y.M. Shin, J.B. Lee, H.J. Sung, O(2) variant chip to simulate site-specific skeletogenesis from hypoxic bone marrow, Sci. Adv. 9 (12) (2023) eadd4210, https://doi.org/10.1126/sciadv.add4210.
[25] S.K. Ramasamy, A.P. Kusumbe, L. Wang, R.H. Adams, Endothelial Notch activity promotes angiogenesis and osteogenesis in bone, Nature 507 (7492) (2014) 376–380, https://doi.org/10.1038/nature13146.
[26] J. Cabanas-Danés, J. Huskens, P. Jonkheijm, Chemical strategies for the presentation and delivery of growth factors, Journal of materials chemistry. B 2 (17) (2014) 2381–2394, https://doi.org/10.1039/c3tb20853b.
[27] K.S. Masters, Covalent growth factor immobilization strategies for tissue repair and regeneration, Macromol. Biosci. 11 (9) (2011) 1149–1163, https://doi.org/10.1002/mabi.201000505.
[28] L. Sheng, Z. Zhang, Y. Zhang, E. Wang, B. Ma, Q. Xu, L. Ma, M. Zhang, G. Pei, J. Chang, A novel "hot spring"-mimetic hydrogel with excellent angiogenic properties for chronic wound healing, Biomaterials 264 (2021) 120414, https://doi.org/10.1016/j.biomaterials.2020.120414.
[29] A. Adini, I. Adini, Z.L. Chi, R. Derda, A.E. Birsner, B.D. Matthews, R.J. D'Amato, A novel strategy to enhance angiogenesis in vivo using the small VEGF-binding peptide PR1P, Angiogenesis. 20 (3) (2017) 399–408, https://doi.org/10.1007/s10456-017-9556-7.
[30] W. Zhao, S.A. McCallum, Z. Xiao, F. Zhang, R.J. Linhardt, Binding affinities of vascular endothelial growth factor (VEGF) for heparin-derived oligosaccharides, Biosci. Rep. 32 (1) (2012) 71–81, https://doi.org/10.1042/bsr20110077.
[31] A. Adini, V.H. Ko, M. Puder, S.M. Louie, C.F. Kim, J. Baron, B.D. Matthews, PR1P, a VEGF-stabilizing peptide, reduces injury and inflammation in acute lung injury and ulcerative colitis animal models, Front. Immunol. 14 (2023) 1168676, https://doi.org/10.3389/fimmu.2023.1168676.
[32] Y. Chen, Z. Yuan, W. Sun, M. Shafiq, J. Zhu, J. Chen, H. Tang, L. Hu, W. Lin, Y. Zeng, L. Wang, L. Zhang, Y. She, H. Zheng, G. Zhao, D. Xie, X. Mo, C. Chen, Vascular endothelial growth factor-recruiting nanofiber bandages promote multifunctional skin regeneration via improved angiogenesis and immunomodulation, Adv. Fiber. Mater. 5 (1) (2023) 327–348, https://doi.org/10.1007/s42765-022-00226-8.
[33] D. Huang, Y. Li, Z. Ma, H. Lin, X. Zhu, Y. Xiao, X. Zhang, Collagen hydrogel viscoelasticity regulates MSC chondrogenesis in a ROCK-dependent manner, Sci. Adv. 9 (6) (2023) eade9497, https://doi.org/10.1126/sciadv.ade9497.
[34] Y. Zhang, Y. Wang, Y. Li, Y. Yang, M. Jin, X. Lin, Z. Zhuang, K. Guo, T. Zhang, W. Tan, Application of collagen-based hydrogel in skin wound healing, Gels. 9 (3) (2023), https://doi.org/10.3390/gels9030185.
[35] W.J. Boyle, W.S. Simonet, D.L. Lacey, Osteoclast differentiation and activation, Nature 423 (6937) (2003) 337–342, https://doi.org/10.1038/nature01658.
[36] G.J. Patti, R. Tautenhahn, G. Siuzdak, Meta-analysis of untargeted metabolomic data from multiple profiling experiments, Nat. Protoc. 7 (3) (2012) 508–516, https://doi.org/10.1038/nprot.2011.454.
[37] J.A. Rasmussen, K.R. Villumsen, M. Ernst, M. Hansen, T. Forberg, S. Gopalakrishnan, M.T.P. Gilbert, A.M. Bojesen, K. Kristiansen, M.T. Limborg, A multi-omics approach unravels metagenomic and metabolic alterations of a probiotic and synbiotic additive in rainbow trout (Oncorhynchus mykiss), Microbiome 10 (1) (2022) 21, https://doi.org/10.1186/s40168-021-01221-8.
[38] G. Cao, J. Liu, H. Liu, X. Chen, N. Yu, X. Li, F. Xu, Integration of network pharmacology and molecular docking to analyse the mechanism of action of Oregano essential oil in the treatment of bovine mastitis, Vet. Sci. 10 (5) (2023), https://doi.org/10.3390/vetsci10050350.
[39] S. Cong, Y. Feng, H. Tang, Network pharmacology and molecular docking to explore the potential mechanism of urolithin A in combined allergic rhinitis and asthma syndrome, Naunyn. Schmiedebergs. Arch. Pharmacol. 396 (9) (2023) 2165–2177, https://doi.org/10.1007/s00210-023-02404-w.
[40] M. Simons, A. Eichmann, Molecular controls of arterial morphogenesis, Circ. Res. 116 (10) (2015) 1712–1724, https://doi.org/10.1161/circresaha.116.302953.
[41] D. Zhao, D. Xiao, M. Liu, J. Li, S. Peng, Q. He, Y. Sun, J. Xiao, Y. Lin, Tetrahedral framework nucleic acid carrying angiogenic peptide prevents bisphosphonate-related osteonecrosis of the jaw by promoting angiogenesis, Int. J. Oral Sci. 14 (1) (2022) 23, https://doi.org/10.1038/s41368-022-00171-7.
[42] Y. Kuroda, T. Kawai, K. Goto, S. Matsuda, Clinical application of injectable growth factor for bone regeneration: a systematic review, Inflamm. Regen. 39 (2019) 20, https://doi.org/10.1186/s41232-019-0109-x.
[43] Z. Qian, H. Li, H. Yang, Q. Yang, Z. Lu, L. Wang, Y. Chen, X. Li, Osteocalcin attenuates oligodendrocyte differentiation and myelination via GPR37 signaling in the mouse brain, Sci. Adv. 7 (43) (2021) eabi5811, https://doi.org/10.1126/sciadv.abi5811.
[44] J. Huang, H. Yin, S.S. Rao, P.L. Xie, X. Cao, T. Rao, S.Y. Liu, Z.X. Wang, J. Cao, Y. Hu, Y. Zhang, J. Luo, Y.J. Tan, Z.Z. Liu, B. Wu, X.K. Hu, T.H. Chen, C.Y. Chen, H. Xie, Harmine enhances type H vessel formation and prevents bone loss in ovariectomized mice, Theranostics. 8 (9) (2018) 2435–2446, https://doi.org/10.7150/thno.22144.
[45] L. Ma, W. Ke, Z. Liao, X. Feng, J. Lei, K. Wang, B. Wang, G. Li, R. Luo, Y. Shi, W. Zhang, Y. Song, W. Sheng, C. Yang, Small extracellular vesicles with nanomorphology memory promote osteogenesis, Bioact. Mater. 17 (2022) 425–438, https://doi.org/10.1016/j.bioactmat.2022.01.008.
[46] Z. Chen, M. Jin, H. He, J. Dong, J. Li, J. Nie, Z. Wang, J. Xu, F. Wu, Mesenchymal stem cells and macrophages and their interactions in tendon-bone healing, J. Orthop. Translat. 39 (2023) 63–73, https://doi.org/10.1016/j.jot.2022.12.005.
[47] A. Wubneh, E.K. Tsekoura, C. Ayranci, H. Uludağ, Current state of fabrication technologies and materials for bone tissue engineering, Acta Biomater. 80 (2018) 1–30, https://doi.org/10.1016/j.actbio.2018.09.031.
[48] M.N. Pantelic, L.M. Larkin, Stem cells for skeletal muscle tissue engineering, Tissue Eng. Part B Rev. 24 (5) (2018) 373–391, https://doi.org/10.1089/ten.TEB.2017.0451.
[49] Y. Xu, X. Zhang, J. You, H. Wang, R. Zheng, L. Wu, L. Tian, J. Guo, F. Fan, Analysis of the cause of cartilage warping in the rhinoplasty of costal cartilage and application of embed-In graft in revisional surgery, Aesthet. Surg. J. 43 (6) (2023) 646–654, https://doi.org/10.1093/asj/sjad011.
[50] X. Wang, D. Zhao, Y. Li, X. Zhou, Z. Hui, X. Lei, L. Qiu, Y. Bai, C. Wang, J. Xia, Y. Xuan, P. Jiang, J. Wang, Collagen hydrogel with multiple antimicrobial mechanisms as anti-bacterial wound dressing, Int. J. Biol. Macromol. 232 (2023) 123413, https://doi.org/10.1016/j.ijbiomac.2023.123413.
[51] W. Zhang, Y. Wu, Q. Chen, H. Zhang, M. Zhou, K. Chen, C. Cao, H. Guo, J. Xu, H. Liu, H. Lin, C. Liu, R. Liu, Statistic copolymers working as growth factor-binding mimics of fibronectin, Adv. Sci. (Weinh) 9 (21) (2022) e2200775, https://doi.org/10.1002/advs.202200775.

[52] S. Zhang, Y. Xie, F. Yan, Y. Zhang, Z. Yang, Z. Chen, Y. Zhao, Z. Huang, L. Cai, Z. Deng, Negative pressure wound therapy improves bone regeneration by promoting osteogenic differentiation via the AMPK-ULK1-autophagy axis, Autophagy. 18 (9) (2022) 2229–2245, https://doi.org/10.1080/15548627.2021.2016231.

[53] R.J. Hinton, Y. Jing, J. Jing, J.Q. Feng, Roles of chondrocytes in endochondral bone formation and fracture repair, J. Dent. Res. 96 (1) (2017) 23–30, https://doi.org/10.1177/0022034516668321.

[54] M.G. Burger, A. Grosso, P.S. Briquez, G.M.E. Born, A. Lunger, F. Schrenk, A. Todorov, V. Sacchi, J.A. Hubbell, D.J. Schaefer, A. Banfi, N. Di Maggio, Robust coupling of angiogenesis and osteogenesis by VEGF-decorated matrices for bone regeneration, Acta Biomater. 149 (2022) 111–125, https://doi.org/10.1016/j.actbio.2022.07.014.

[55] D.V. Novack, S.L. Teitelbaum, The osteoclast: friend or foe? Annu Rev. Pathol. 3 (2008) 457–484, https://doi.org/10.1146/annurev.pathmechdis.3.121806.151431.

[56] Y. Han, X. You, W. Xing, Z. Zhang, W. Zou, Paracrine and endocrine actions of bone-the functions of secretory proteins from osteoblasts, osteocytes, and osteoclasts, Bone Res. 6 (2018) 16, https://doi.org/10.1038/s41413-018-0019-6.

[57] M. Wu, H. Liu, D. Li, Y. Zhu, P. Wu, Z. Chen, F. Chen, Y. Chen, Z. Deng, L. Cai, Smart-responsive multifunctional therapeutic system for improved regenerative microenvironment and accelerated bone regeneration via mild photothermal therapy, Adv. Sci. (Weinh) 11 (2) (2024) e2304641, https://doi.org/10.1002/advs.202304641.

[58] M. Wu, H. Liu, Y. Zhu, P. Wu, Y. Chen, Z. Deng, X. Zhu, L. Cai, Bioinspired soft-hard combined system with mild photothermal therapeutic activity promotes diabetic bone defect healing via synergetic effects of immune activation and angiogenesis, Theranostics. 14 (10) (2024) 4014–4057, https://doi.org/10.7150/thno.97335.